



Performance analysis of solar assisted heat pump coupled with build-in PCM heat storage based on PV/T panel

Yao, J., Xu, H., Dai, Y., & Huang, M. (2020). Performance analysis of solar assisted heat pump coupled with build-in PCM heat storage based on PV/T panel. *Solar Energy*, 197, 279-291.
<https://doi.org/10.1016/j.solener.2020.01.002>

[Link to publication record in Ulster University Research Portal](#)

Published in:
Solar Energy

Publication Status:
Published (in print/issue): 01/02/2020

DOI:
[10.1016/j.solener.2020.01.002](https://doi.org/10.1016/j.solener.2020.01.002)

Document Version
Author Accepted version

General rights

Copyright for the publications made accessible via Ulster University's Research Portal is retained by the author(s) and / or other copyright owners and it is a condition of accessing these publications that users recognise and abide by the legal requirements associated with these rights.

Take down policy

The Research Portal is Ulster University's institutional repository that provides access to Ulster's research outputs. Every effort has been made to ensure that content in the Research Portal does not infringe any person's rights, or applicable UK laws. If you discover content in the Research Portal that you believe breaches copyright or violates any law, please contact pure-support@ulster.ac.uk.

Manuscript Number: SE-D-19-01268R3

Title: Performance analysis of solar assisted heat pump coupled with
build-in PCM heat storage based on PV/T panel

Article Type: VSI:Solar Integration

Keywords: PV/T; Solar energy; Heat pump; Build-in PCM heat storage;
Heating/Power generation; Residential heating

Corresponding Author: Professor Yanjun DAI, Ph.D

Corresponding Author's Institution: Shanghai Jiao Tong University

First Author: Jian YAO

Order of Authors: Jian YAO; Hui XU; Yanjun DAI, Ph.D; Mingjun HUANG

Manuscript Region of Origin: CHINA

Abstract: PV/T (photovoltaic/thermal) technology is a combination of PV module (photovoltaic utilization) and collector (photothermal utilization), which can improve the comprehensive utilization efficiency of solar energy and has a broad application prospect. In this paper, PV/T module is coupled with heat pump evaporator to form a direct-expansion solar PV/T heat pump which is suitable for heat application in high latitude area. To achieve stable residential heating, a solar PV/T heat pump system coupled with build-in PCM (phase change material) heat storage is therefore proposed and simulated. Meanwhile, the mathematical model of solar PV/T heat pump coupled with build-in PCM heat storage system is established and verified. The simulation results show that the temperature of underfloor heating which using build-in PCM heat storage can reach 22 °C to 31 °C after 39 hours when the circulating water is 40 °C. Moreover, the heating COP (Coefficient of Performance) increases with the increase of solar radiation, ambient temperature and area of PV/T collector, and decrease of wind speed, respectively. A 20 m² PV/T panel module can output 21.4% of the electricity to power grid when the solar radiation intensity is 600 W/m² and meet the heat demand of a 100 m² room while maintain the operation of the system. Meanwhile, the heating COP can reach 5.79 which is 70% higher than the conventional air conditioning system and the electrical, thermal, overall efficiencies are 17.77%, 55.76% and 75.49%, respectively.

Highlights

- A solar assisted heating/power generation system based on PV/T panel is proposed for residential heating in high latitude area.
- Design of build-in PCM heat storage unit is proposed and simulated.
- The comprehensive energy utilization efficiency of this solar PV/T heat pump system can reach above 75%.

Dear editor and reviewers:

Thanks for your responsible comments on our manuscript. It is very valuable and helpful to improve our paper. We have revised the manuscript carefully according to your suggestions. The revised portions are marked in red in the revised manuscript.

Reviewer 1

#1. The validation process are wrong. Firstly, the system reported in the manuscript is totally different from the validation case, which comes from the last Reference, Zhou et al. 2019. In Zhou's study, there is no any pcm thermal energy storage (PCM-TES) unit, while the PCM-TES unit in this study is the novelty in the system. By using different system to validate this work, it is hardly possible to get reasonable results, even the given data seems agree well.

Response: Thanks for your comments. As shown in Fig. 2, the solar PV/T heat pump cycle is the main sub cycle of the proposed system. In Zhou's paper, they proposed a solar PV/T heat pump system which has the same components (PV/T collector/evaporator, compressor, condenser, expansion valve). The only difference between Zhou's paper and our proposed system is that in our proposed system, the thermal energy will be stored in build-in PCM heat storage unit, but in Zhou's system, it will be stored directly in hot water tank. In other words, the difference is just the type of heat storage, in PCM-TES or in water tank. Therefore, the added PCM-TES unit in our proposed system will not influence the performance of solar PV/T heat pump system (For example, thermodynamic state points of each components, thermal energy gain through PV/T panel, heat of condensation, etc.). It's reasonable to refer Zhou's experiments results for validation due to the same basic thermodynamic cycle and operating conditions.

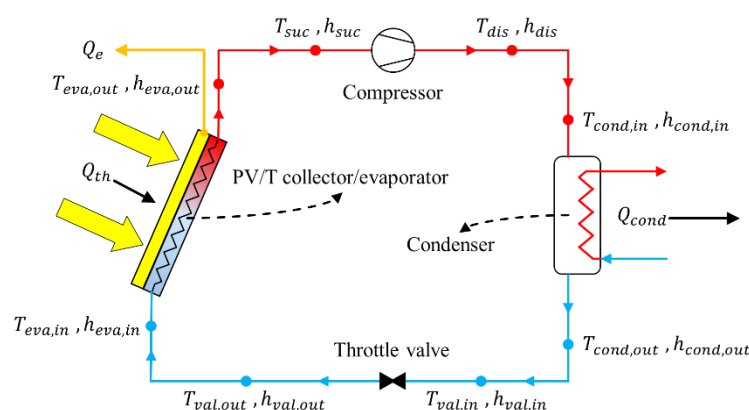


Fig. 2. The thermodynamic state points for each component.

#2. In Fig. 12, there is simulated photovoltaic efficiency. How to simulate it? It is totally influences by the material and structure of the PV panel. It seems hardly possible to simulate its performance. Furthermore, even there is some semi-empirical calculated data, it can not be used to validate the coupled system reported in this study. Only by using the same system, the model could be validated. It seems common sense.

Response: Thank you for your comments. According to Huide's paper, the photovoltaic efficiency can be calculated by Eq. (2). η_{rc} is the reference photovoltaic efficiency value of the PV cells at $T_{rc}=298\text{ K}$, $I=1000\text{ W/m}^2$, $\eta_{rc}=0.18$; β_{pv} is the temperature coefficient (1/K) of PV cell efficiency, $\beta_{pv}=0.0045$ (Huide et al., 2017).

$$\eta_e = \eta_{rc} \cdot \left[1 - \beta_{pv} \cdot (T_p - T_{rc}) \right] \quad (2)$$

As shown in Eq. (2), the reference photovoltaic efficiency (η_{rc}) is determined by material and structure of PV panel. However, the photovoltaic efficiency (η_e) is only influenced by PV cells' temperature (T_p) which could be simulated when the material and structure is fixed.

The simulation process of PV cells' temperature is as follows: firstly, input all the environmental, system design, operation parameters and assume the temperature of PV cells (T_p). Secondly, calculate the overall heat loss rate (Q_L), PV electrical output power (Q_e), thermal energy gain rate through PV/T collector/evaporator (Q_{th}) and the useful heat transfer rate by refrigerant (Q_u). Then the program starts iteration and moves to next step when $|(Q_{th} - Q_u)/Q_{th}| < 0.1\%$ which means the system achieves energy balance. If $|(Q_{th} - Q_u)/Q_{th}| \geq 0.1\%$, the PV cells' temperature (T_p) would be modified and the program would start another iteration using the modified T_p . Thus, the PV cells' temperature could be calculated through the program as well as the photovoltaic efficiency. The algorithm has been presented in section 3.5.

The proposed system has the same thermodynamic cycle and operating conditions with Zhou's study which consist of PV/T collector/evaporator, compressor, condenser, expansion valve. Compared to Zhou's system, the only difference is that the proposed system has added a thermal storage part which will not influence the heat pump system's performance. Thus, the proposed solar PV/T heat pump system could be validated by Zhou's system.

#3. There are too many figures and tables are useless in this manuscript, which makes this manuscript long and even dull. For example, Fig. 3c is not mentioned at all.

I do know why authors use the solar radiation intensity data in Figs. 11 and 12, but not mentioned them at all. This makes the figures much more complex.

Response: Thank you for your comments. The authors have revised the manuscript, several figures have been deleted and Fig. 11, Fig. 12 have been modified. The revised figures are listed as follows:

1. Fig. 3 (c)(d) have been deleted.
2. Fig. 8 (c~l) have been deleted.
3. Fig. 26 has been deleted.
4. Fig. 11 and Fig. 12 have been revised to Fig. 11. (a)(b) according to your comments. The curves of solar radiation intensity have been deleted in revised Fig. 11. (a)(b) and these two figures are simpler and easier to understand.

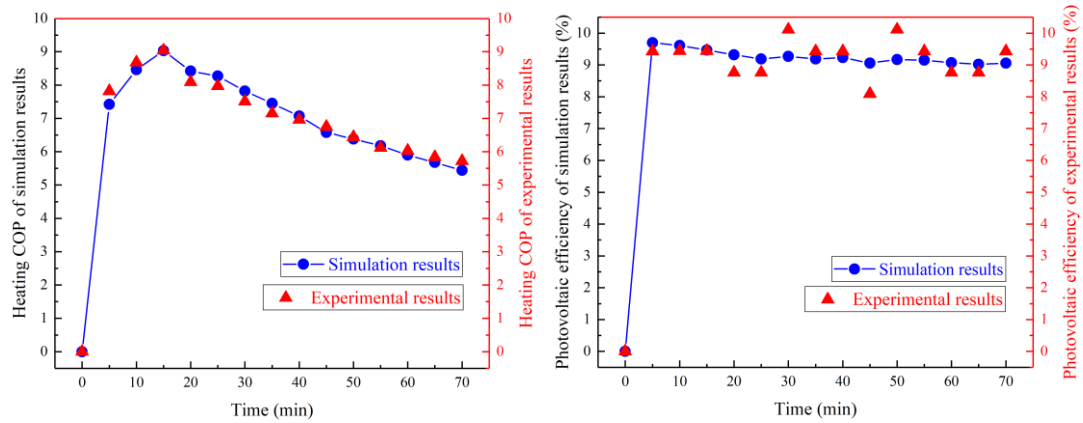


Fig. 11. (a) Comparison results of experimental and simulated heating COP. (b) Comparison results of experimental and simulated photovoltaic efficiency.

#4. Many unimportant results are given in the conclusions, such as the following one.

(2) The heating COP increases with the increase of solar radiation, ambient temperature, area of PV/T collector, and decrease of wind speed, respectively. Solar radiation intensity and area of PV/T collector are two major factors affecting system performance compared to wind speed and ambient temperature.

As far as I know, this conclusion could be given even this work is not conducted. It could be given easily. Clearly, the novelty of this work is lack.

Response: Thank you for your comments. The second conclusion in Line 625-628 has been deleted according to your comments. The novelty of this work has been added in section Introduction in Line 102-104.

The revised manuscript of Line 102-104 is as follows:

The objective of this paper is to provide a promising method to realize stable, high efficiency, environmental friendly residential heating in high latitude area with no energy consumption from power grid.

#5. Even authors revised the manuscript many times, there are still many problems. For example, in Fig.8, the color bar starts at different temperatures, 290 K, 300 K, 287 K, 297 K, etc. Why?

Response: Thank you for your comments. According to your Comment #3, Fig. 8 (c~l) have been deleted. The color bar starts at the same temperature in revised Fig. 8 (a)(b)(c).

The revised manuscript of Fig. 8 is as follows:

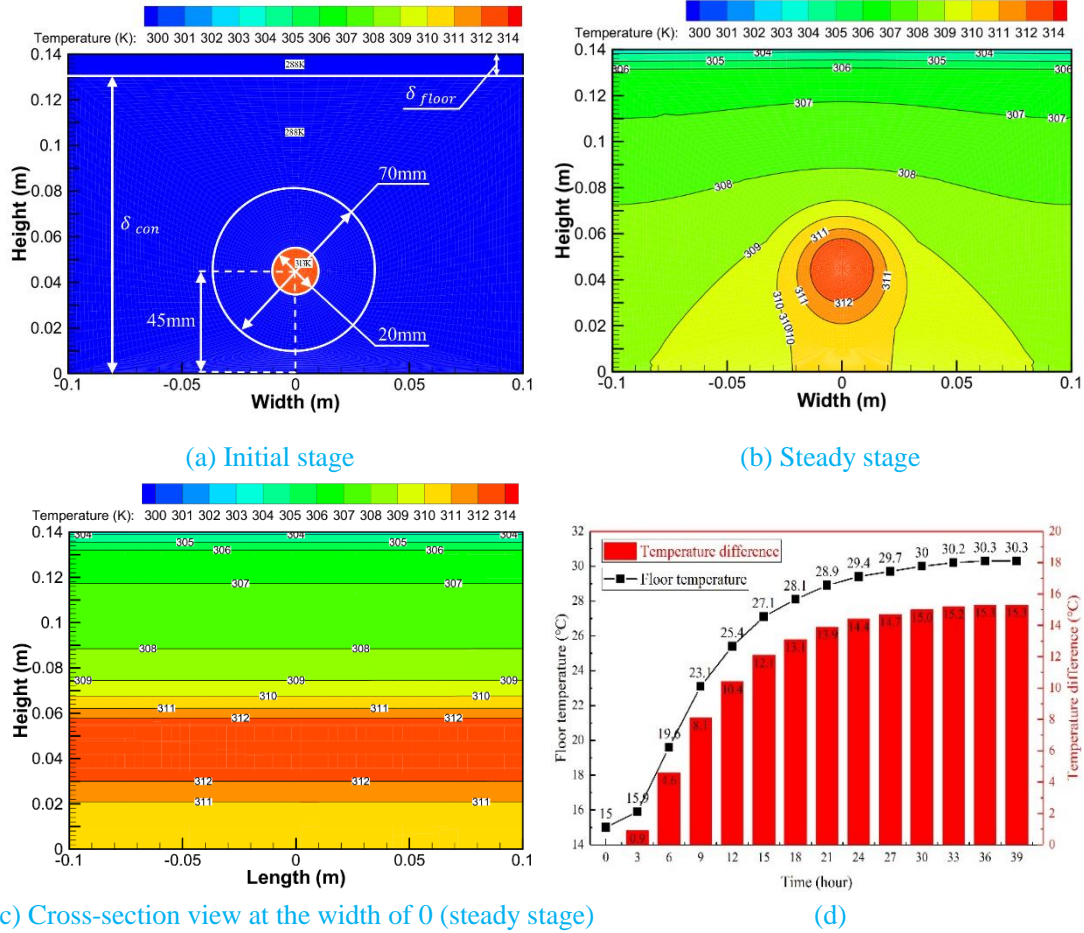


Fig. 8. (a~c) Cross-section temperature contour of the build-in PCM heat storage unit at initial and steady stage. (d) Variation curve of floor temperature and temperature difference between floor and ambient.

#6. The manuscript has a poor structure, and the length could be divided into 2-3 articles. It is hard to make reader understand the main goal of this work from this manuscript.

Response: Thank you for your comments.

Our structure for writing this article is as follows: we firstly propose the solar PV/T heat pump system coupled with build-in PCM heat storage. Then, we design and evaluate the build-in PCM heat storage. Next, we therefore investigate the performance of solar PV/T heat pump system coupled with PCM-TES. Finally, we conduct the feasibility analysis and merits of the proposed system.

The main goal of this paper which has been added in Line 102-104 is to provide a promising method to realize stable, high efficiency, environmental friendly residential heating in high latitude area with no energy consumption from power grid.

According to your comments, several paragraphs have been deleted. The revised parts in manuscript are as follows:

1. Line 104-106.
2. Line 160-161.
3. Line 164-165.

4. Line 248-255.
5. Line 303-308.
6. Line 606-611.
7. Line 625-628.

Reviewer 5

The authors have made clear responses. Now the present manuscript is acceptable for publication.

Response: Thank you for your comments.

Performance analysis of solar assisted heat pump coupled with build-in PCM heat storage based on PV/T panel

Jian YAO ^{a, b}, Hui XU ^{a, b}, Yanjun DAI ^{a, b, *}, Mingjun HUANG ^c

^a Institute of Refrigeration and Cryogenics, Shanghai Jiao Tong University, Shanghai 200240, China

^b Engineering Research Center of Solar Power and Refrigeration, MOE, China

^c Centre for Sustainable Technologies, School of the Built Environment, University of Ulster, Newtownabbey, Northern Ireland, BT37 0QB, UK

E-mail address: yjdai@sjtu.edu.cn (Yanjun DAI); Tel.: +86-21-34204358; fax: +86-21-34206814

Abstract

PV/T (photovoltaic/thermal) technology is a combination of PV module (photovoltaic utilization) and collector (photothermal utilization), which can improve the comprehensive utilization efficiency of solar energy and has a broad application prospect. In this paper, PV/T module is coupled with heat pump evaporator to form a direct-expansion solar PV/T heat pump which is suitable for heat application in high latitude area. To achieve stable residential heating, a solar PV/T heat pump system coupled with build-in PCM (phase change material) heat storage is therefore proposed and simulated. Meanwhile, the mathematical model of solar PV/T heat pump coupled with build-in PCM heat storage system is established and verified. The simulation results show that the temperature of underfloor heating which using build-in PCM heat storage can reach 22 °C to 31 °C after 39 hours when the circulating water is 40 °C. Moreover, the heating COP (Coefficient of Performance) increases with the increase of solar radiation, ambient temperature and area of PV/T collector, and decrease of wind speed, respectively. A 20 m² PV/T panel module can output 21.4% of the electricity to power grid when the solar radiation intensity is 600 W/m² and meet the heat demand of a 100 m² room while maintain the operation of the system. Meanwhile, the heating COP can reach 5.79 which is 70% higher than the conventional air conditioning system and the electrical, thermal, overall efficiencies are 17.77%, 55.76% and 75.49%, respectively.

1 Introduction

The total amount of energy consumption in the world is constantly climbing (2019; Caetano et al., 2017). The consumption of fossil energy has brought about energy crisis and environmental crisis (Pietrosemoli and Rodríguez-Monroy, 2019). Without action, CO₂ emissions from burning fossil fuels will be doubled by 2050 (Paolo Frankl, 2010). Therefore, the development and utilization of renewable energy has become one of the effective solutions (Keček et al., 2019). Solar energy has become the first choice due to its characteristics of ubiquity, abundance and sustainability (Kuik et al., 2019; Tsai, 2015), which is mainly used in two ways: photothermal and photovoltaic. 11% of global electricity will be provided by PV by 2050 (Paolo Frankl, 2010). However, the electrical efficiency of PV cells decreases with the increase of the temperature of PV cells (Huide et al., 2017). A cooling system can be added to reduce the temperature of PV cells while the remaining heat of PV panel are absorbed by working fluid which can be employed as a useful thermal energy for heat applications in buildings.

The PV/T technology coupled PV modules with thermal collectors was first proposed by Wolf et al (Wolf, 1976) to reduce PV cells temperature and improve electrical efficiency. The PV/T system can recover waste heat from the PV panel to improve comprehensive energy utilization efficiency. PV/T design optimizations are carried out to improve the system efficiency in recent years. Nahar et al. (Nahar et al., 2017) designed a novel pancake-shaped flow channel for PV/T system, and integrated the flow channel with the PV baseboard. They found that the temperature of the PV panel is reduced by 42 °C, and the electrical efficiency is increased by 2%. Othman et al. (Othman et al., 2016) proposed a parallel, double pass flat plate collector which was adopted in a two fluids PV/T system. Their results showed that the electrical efficiency and thermal efficiency are 17% and 76%, respectively.

The combination of PCM and PV/T panel is an effective way to stabilize the operating temperature of PV cells and improves the overall efficiency. Hosseinzadeh et al. (Hosseinzadeh et al., 2018) investigated the effect of simultaneous use of nanofluid as coolant as well as an organic paraffin as the phase change material on the electrical and thermal efficiencies. They demonstrated that the use of PCM in nanofluid based PVT/PCM system enhances the thermal output power of conventional PV/T system by 29.6%. Kazemian et al. (Kazemian et al., 2019) developed and simulated a comprehensive three-dimensional model of PV/T system integrated with PCM. Their simulation results presented that the PV/T-PCM system have lower surface temperature compared to PV/T system, and as the thermal conductivity of PCM enhances, both electrical and thermal efficiencies increase. Fayaz et al. (Fayaz et al., 2019) investigated the PCM based PV/T system, and the experimental validation was carried out to verify the numerical model. They found that the electrical efficiency is achieved as 13.98% and 13.87% numerically and experimentally respectively, and the electrical performance is improved as 6.2% and 4.8% for PV/T-PCM system based on the numerical and experimental results respectively.

Different working fluids like water, air, nanofluid and refrigerant are also used to cool the PV module. Huang and Lee (Huang and Lee, 2004) conducted long-term tests on the direct-expansion solar heat pump which adopted refrigerant as working fluid to verify the stability of the work. The total running time of their prototype is over 20000 hours, and the measured energy consumption is 0.019 kWh/l of hot water at 57 °C which is much less than traditional solar water heater. Stojanović and Akander (Stojanović and Akander, 2010) used direct-expansion heat pump for independent buildings heating and domestic hot water supply. In their system, the collector area is 42.5 m² and heat pump power is 8.4 kW, they measured that the actual indoor temperature is no less than 20 °C during the testing period. Alejandro Del Amo et al. (Del Amo et al., 2019) verified the feasibility of solar PV/T heat pump through experiments. They obtained that the highest COP of the system can reach 4.62. Meanwhile, the PV module provides 67.6% of the power demand, and the payback period is 6 years.

In addition to optimize the PV/T panel, the adoption of PCM as heat storage is also a good way to stabilize the system. Kuznik et al. (Kuznik et al., 2008) adopted PCM wallboard heat storage and conducted comparative experiments. In their study, the system can effectively reduce heat loss, keep the room warm and improve indoor thermal comfort. Fiorentini et al. (Fiorentini et al., 2015) combined PCM storage with PV/T system, and the roof was used as PV/T layout location. The PCM storage adopted in their system can keep indoor comfort within a certain and potentially variable thermal comfort range. Diallo et al. (Diallo et al., 2019) proposed the PVT-LHP (PVT Loop Heat Pipe) technology employing PCM triple heat exchanger, the total

energy efficiency of the presented system is improved by 28%, and the heating COP is 2.2 times than that of a traditional PV/T system.

Owing to the instability of solar energy, traditional solar PV/T system cannot continuously and stably supply heat or power generation when solar irradiation is weak such as rainy day or winter. Consequently, the market of PV/T technology compared with PV or PT system is still very low. PV/T can adapt to the characteristics of low intensity, instability and intermittency of solar energy better if it can be combined with accumulator and heat storage. However, additional space is required to install heat storage tank, which is not suitable for use in urban areas where land resources are scarce. Therefore, in this paper, a coupling design of solar PV/T heat pump and build-in PCM heat storage is proposed and the parallel air source heat exchanger is also adopted to enhance the stability of the system. The build-in PCM heat storage used for underfloor heating is a combination of PCM and building materials, which can save more space compared to conventional PCM storage tank system. Firstly, the composition and operation modes of the system are introduced. According to the system principle, the mathematical model is established and verified, and the build-in PCM heat storage sub-system which using for residential heating is also proposed and simulated. Then the influences of different parameters on system performance are analyzed. Finally, the feasibility analysis of the system is conducted. The objective of this paper is to provide a promising method to realize stable, high efficiency, environmental friendly residential heating in high latitude area with no energy consumption from power grid.~~The proposed and calculated analysis of the scheme is conducive to assisting in the design and optimization of the solar PV/T heat pump system coupled with build-in PCM heat storage.~~

2 System description

Fig. 1 shows the schematic diagram of the system based on solar PV/T heat pump, which is consisted of four main parts: solar PV/T heat pump module, parallel air source heat pump module, heat storage module and electrical module. The blue lines represent low temperature working fluid, and in the opposite, red lines represent high temperature. The yellow lines represent the electricity flow direction. The arrows show the working fluid direction. The system can be divided into two operating modes, which are listed as follows.

(1) Sunny day operating mode: The electricity generated by PV panel is used to drive the pumps and compressor, and the excess electricity will be recovered to the power grid or drive the air conditioning. However, the PV panel heated by solar radiation will be resulted in an increase of the temperature of PV cells. Meanwhile, the heat transferred by the PV/T collector can be absorbed by the refrigerant. Then, the superheated refrigerant vapor with low pressure is compressed by the compressor to the high temperature and pressure refrigerant vapor. The condensation heat will be absorbed and stored in the build-in PCM heat storage. The heat transferred by condensation can also be used for producing domestic hot water. The liquid refrigerant will expand through the throttle valve after condensation process, and flow into the PV/T collector/evaporator. The heat released from the heat storage module will be used to keep the indoor temperature constant during the night.

(2) Rainy day operating mode: The system will switch to the air source heat pump mode when the solar radiation is insufficient to maintain system operation. The pumps and compressor driven by power grid are used to keep the system work. The air fan heat exchanger is adopted to absorb heat from the ambient air. The refrigerant will be heated by the air fan heat exchanger and

compressed by compressor into high temperature and pressure vapor. The heat released by the refrigerant vapor will be transferred to the PCM or water. This mode can make full use of the valley electricity to store heat at night, and maintain the indoor temperature through the heat storage module during the day.

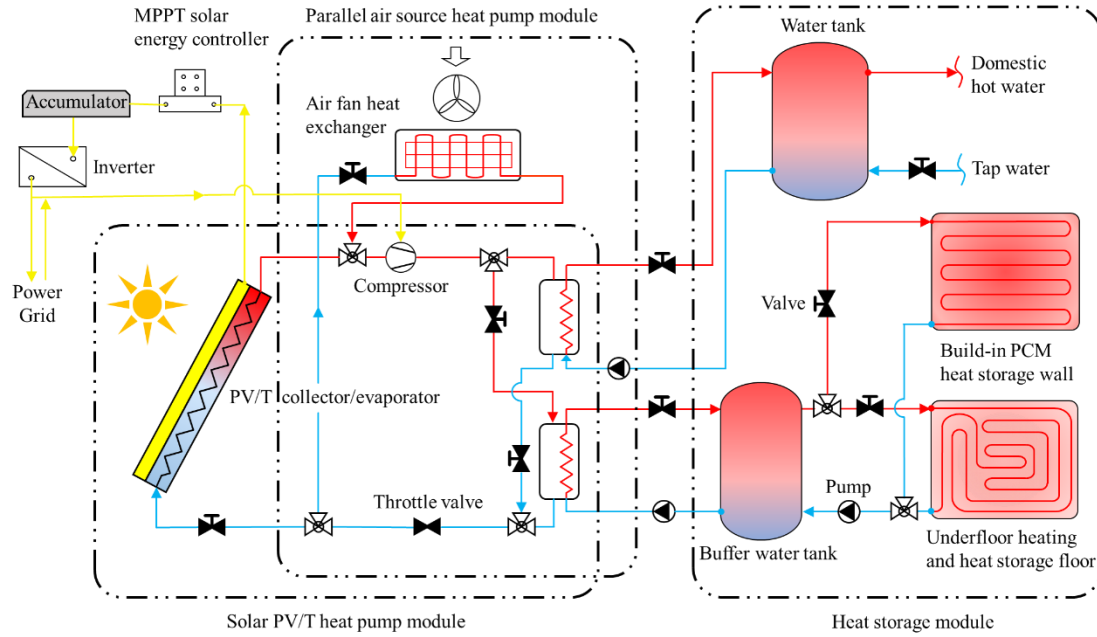


Fig. 1. Schematic of the system based on solar PV/T heat pump.

3 Mathematical model

The thermodynamic state points for each process are shown in Fig. 2. The solar PV/T heat pump cycle could be simplified to four components: PV/T collector/evaporator, compressor, PCM heat exchanger and throttle valve. Different temperature (T) and enthalpy (h) at each state point are shown in Fig. 2. Q_{th} (W) is the heat transfer rate between refrigerant and the PV/T panel, Q_e (W) is the electrical power provided by PV panel, and Q_{PCM} (W) is the heat transfer rate between refrigerant and phase change materials.

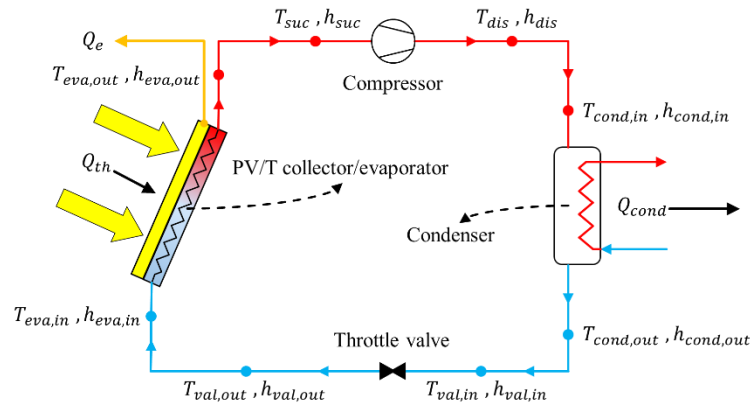


Fig. 2. The thermodynamic state points for each component.

The design parameters of the system and characteristics of different PV/T layers are listed in Table. 1.

Table. 1. Design parameters of the system and characteristics of different PV/T layers.

Parameters	Nomenclature	Value	Unit
Thickness of PV-glazing cover	$\delta_{g,pv}$	1	mm
Emissivity of PV-glazing cover	ε_c	0.84	[-]
Transmissivity of PV-glazing cover	$\tau_{g,pv}$	0.9	[-]
Thickness of PV cells	δ_{pv}	0.3	mm
Emissivity of PV cells	ε_p	0.96	[-]
Absorptance of PV cells	a_p	0.85	[-]
Thermal conductivity of PV cells	κ_p	203	W/m·K
Absorptance of PV baseboard	a_b	0.8	[-]
Thickness of EVA grease	δ_{EVA}	0.5	mm
Thermal conductivity of EVA grease	κ_{EVA}	0.311	W/m·K
Thickness of electrical insulation	δ_{ei}	0.5	mm
Thermal conductivity of electrical insulation	κ_{ei}	0.15	W/m·K
Electrical insulation material	[-]	Tedlar	[-]
Packing factor	β_p	1	[-]
Length of PV/T collector/evaporator	L	2.0	m
Width of PV/T collector/evaporator	W	1.0	m
Area of the PV/T collector/evaporator	A	2.0	m ²
Thermal conductivity of roll-bond panel	κ_{rb}	151	W/m·K
Thickness of roll-bond panel pipe	δ_{rb}	1	mm
Refrigerant type	ref	R134A	[-]

3.1. Model of PV/T collector/evaporator

The heat absorbed by the PV/T panel is expressed as follows:

$$Q_{abs} = (1 - \eta_e) \cdot A \cdot I \cdot \tau_{g,pv} \cdot [\alpha_p \cdot \beta_p + \alpha_b \cdot (1 - \beta_p)] \quad (1)$$

where A is the collector area of the PV/T panel (m²); I is the solar radiation intensity (W/m²); $\tau_{g,pv}$ is the transmittances of the PV-glazing cover; a_p and a_b are the absorption ratios of the PV cells and its baseboard, respectively; β_p is the packing factor of PV cells; η_e is the PV cells' efficiency, calculated by (Huide et al., 2017):

$$\eta_e = \eta_{rc} \cdot [1 - \beta_{pv} \cdot (T_p - T_{rc})] \quad (2)$$

η_{rc} is the reference photovoltaic efficiency value of PV cells at $T_{rc}=298$ K, $\eta_{rc}=0.18$; β_{pv} is the temperature coefficient (1/K) of PV cell efficiency, $\beta_{pv}=0.0045$ (Huide et al., 2017).

~~The heat loss, physical model of the PV/T collector/evaporator, the front view of PV/T panel on the roof and the roll bond panel which encapsulated in the PV/T panel are shown in Fig. 3. Fig. 3 shows the heat loss and physical model of PV/T panel which has a multi-layer structure, the heat loss of PV/T panel consists of two parts: (1) heat transfer from PV cells to PV-glazing cover; (2) heat transfer from PV-glazing cover to ambient air. The thermal resistances of the PV/T module are shown in Fig. 3(a), and all consist of convection and radiation thermal resistance in different part.~~

The total heat loss rate of PV/T module is given as:

$$Q_L = U_L \cdot A \cdot (T_p - T_a) \quad (3)$$

where T_p and T_a are the temperature of PV cells and ambient air, respectively. U_L is the overall heat loss coefficient which can be written as:

$$U_L = \left[1 / (h_{cv,p-c} + h_{rd,p-c}) + 1 / (h_{cv,c-a} + h_{rd,c-a}) \right]^{-1} \quad (4)$$

$h_{cv,p-c}$ and $h_{rd,p-c}$ are the convective and radiative heat-transfer coefficients between PV cells and glass cover; $h_{cv,c-a}$ and $h_{rd,c-a}$ are the convective and radiative heat-transfer coefficients between glass cover and ambient.

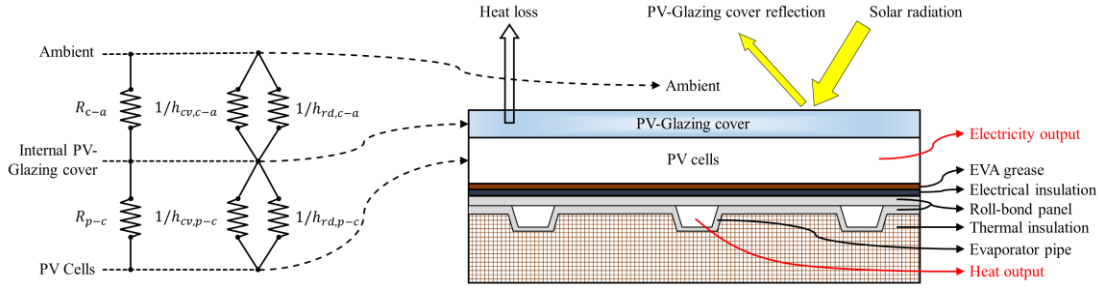


Fig. 3. Heat loss and physical model of PV/T collector/evaporator.



Fig. 3. (a) Heat loss of the PV/T collector/evaporator. (b) Physical model of the PV/T collector/evaporator. (c) Front view of PV/T panel on the roof. (d) Roll bond panel.

The overall electricity output power of PV cells is given as:

$$Q_e = A \cdot I \cdot \tau_{g,pv} \cdot \alpha_p \cdot \beta_p \cdot \eta_e \quad (5)$$

Under the steady-state condition, the heat transfer rate delivered by the module equals the rate of the absorbed heat minus the overall heat loss, expressed as:

$$Q_{th} = Q_{abs} - Q_L \quad (6)$$

The total useful solar heat received by the PV/T collector/evaporator is expressed as:

$$Q_u = F_R \cdot A \cdot I \cdot \tau_{g,pv} \cdot \left[\alpha_p \cdot \beta_p + \alpha_b \cdot (1 - \beta_p) \right] \quad (7)$$

where F_R is the PV/T collector thermal efficiency factor, can be defined as (Diallo et al., 2019):

$$F_R = (1 - \eta_e) \cdot \frac{1/U_L}{L \cdot W / N_{rb} \cdot \left\{ 1 / \left(L \cdot U_L - \left[(W / N_{rb} - L_{rb}) F_{rb} + L_{rb} / (1 + R_{pv} \cdot U_L) \right] \right) + \sum_1^5 R_i \right\}} \quad (8)$$

N_{rb} is the equivalent number of roll-bond panel pipe; L_{rb} is the equivalent length of roll-bond panel pipe; $\sum R_i$ is the overall thermal resistance from the PV cells to the PCM; F_{rb} is the efficiency of the roll-bond panel which encapsulated in the backside of the PV/T panel which can be defined as (Diallo et al., 2019):

$$F_{rb} = \tanh \left[\frac{\sqrt{\frac{U_L}{k_{rb} \delta_{rb} (1 + R_{pv} U_L)}} (W / N_{rb} - L_{rb}) / 2}{\sqrt{\frac{U_L}{k_{rb} \delta_{rb} (1 + R_{pv} U_L)}} (W / N_{rb} - L_{rb}) / 2} \right] \quad (9)$$

k_{rb} is the thermal conductivity of roll-bond panel; δ_{rb} is the thickness of the roll-bond panel pipe; R_{pv} is the thermal resistance of PV cells.

The thermal resistances of the PV/T system and heat transfer along the system are shown in Fig. 4.

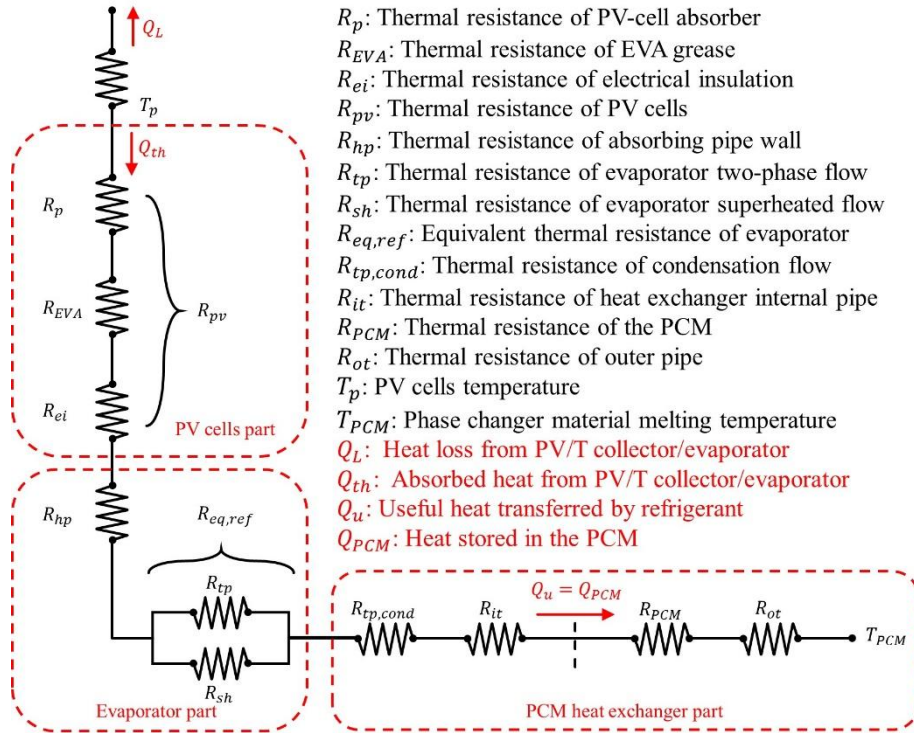


Fig. 4. Thermal resistances of the PV/T system and heat transfer along the system.

Heat transfer between PV module and heat pipe is a conventional one dimensional heat conduction process and its associated thermal resistance is:

$$R_{pv} = \delta_p / k_p + \delta_{EVA} / k_{EVA} + \delta_{ei} / k_{ei} \quad (10)$$

Superheated region and two-phase region existed in the refrigerant side of the PV/T collector/evaporator. The equivalent thermal resistance of the two different regions can be calculated as (P. Hartnett and M. Rohsenow, 1973):

$$R_{eq,ref} = \left(1 / R_{tp} + 1 / R_{sh} \right)^{-1} \quad (11)$$

3.2. Model of build-in PCM heat storage

All the heat gained by the build-in PCM heat storage is transferred by the PCM heat exchanger. The heat store rate in the PCM and concrete is expressed as follows:

$$Q_{PCM} + Q_{conc} = \dot{m}_{ref} \cdot (h_{dis} - h_{in}) \quad (12)$$

The PCM melting rate is calculated by:

$$\dot{m} = Q_{PCM} / \Delta H_{PCM} \quad (13)$$

where ΔH_{PCM} is the latent heat of the PCM (kJ/kg).

Fig. 5 shows the phase change temperature of 15 kinds of phase change materials including organic/inorganic/eutectic compounds materials. According to L.F. Cabeza et al. (Cabeza et al., 2011), the recommendation phase change temperature range for underfloor heating is between 30 °C to 40 °C. There are five kinds of PCM that have phase change temperature in this range:

Paraffin wax, $\text{CaCl}_2 \cdot (\text{H}_2\text{O})_6$ - $\text{MgCl}_2 \cdot (\text{H}_2\text{O})_6$, Calcium chloride hexahydrate, Sodium sulphate decahydrate, Sodium phosphate dibasic dodecahydrate.

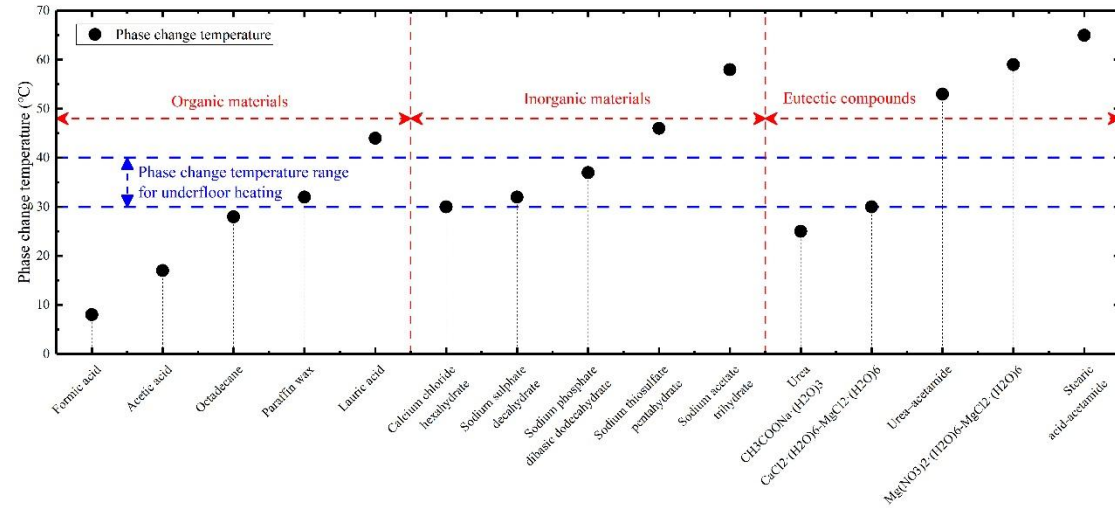
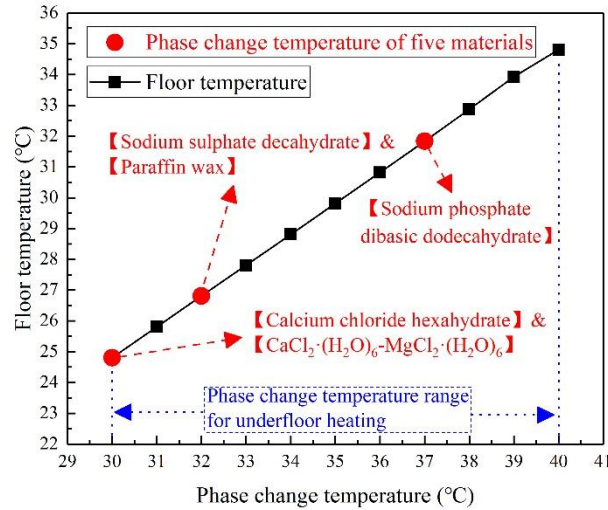


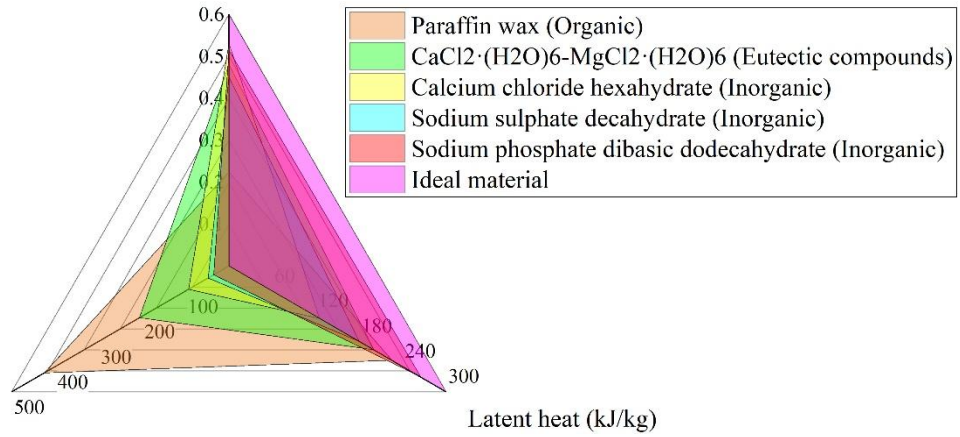
Fig. 5. Phase change temperature of 15 kinds of PCM including Organic/Inorganic/Eutectic compounds materials.

The variation curve of floor temperature with phase change temperature and the comparison of three indices including thermal conductivity, latent heat and price (Pereira da Cunha and Eames, 2016) of above five kinds of PCM are shown in Fig. 6. These five materials have different phase change temperature which all in the recommendation temperature range for underfloor heating. The ideal material should have a higher thermal conductivity and latent heat while the price is low. In order to evaluate these five materials, the graph of ideal material is also plotted in Fig. 6. The organic and eutectic compounds phase change materials have a higher price than inorganic materials while the thermal conductivity and latent heat are lower. Moreover, the larger of the overlap area in Fig. 6 between each material and ideal material, the better of the material performance. As shown in Fig. 6, Sodium phosphate dibasic dodecahydrate has the largest overlap area, thus, it is used in the simulation of build-in PCM heat storage unit.



(a)

Thermal conductivity (W/m·K)



(b)

Fig. 6. (a) Variation curve of floor temperature with phase change temperature. **(b)** Thermal conductivity/Latent heat/Price comparison of six kinds of materials including ideal material.

Fig. 7 illustrates the structure and cross-section view of a build-in PCM heat storage unit which is the component of underfloor heating module. The phase change materials (Sodium phosphate dibasic dodecahydrate) are placed in the outer tube of a double-wall tube which can store heat during the day and release latent heat at night. The floor temperature range of the underfloor heating is 20 °C to 35 °C for residential applications. The phase change materials should have a melting temperature lying in the practical range of operation, melt congruently with minimum subcooling and be chemically stable, low in cost, nontoxic and non-corrosive. Moreover, as shown in Fig. 8(b), the outer tube of the build-in PCM heat storage is around 37 °C when the circulating water temperature is 40 °C. Thus, it is reasonable to choose a phase change material which melting point is around 37 °C. The cross-section view of the build-in heat storage unit is shown in Fig. 7(b). Polystyrene board and foam concrete are used as thermal insulation and building materials, respectively. The hot water which produced by solar PV/T heat pump module is pumped into the pipe of underfloor heating to keep the indoor temperature steady. The properties of PCM (Jankowski and McCluskey, 2014) and concrete as well as underfloor heating

working conditions are listed in Table. 2.

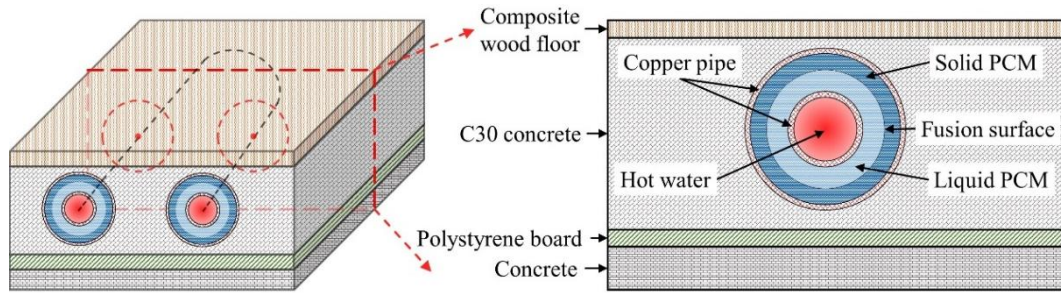
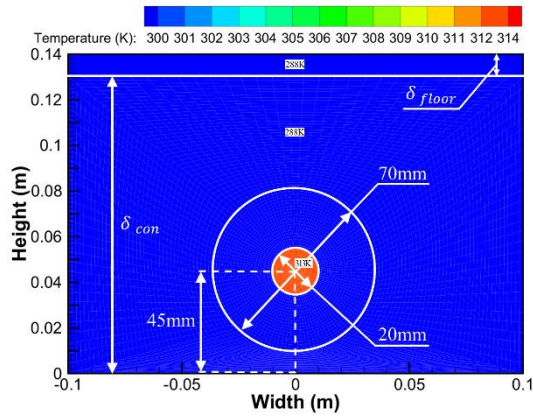


Fig. 7. Structure and cross-section view of the build-in PCM heat storage unit.

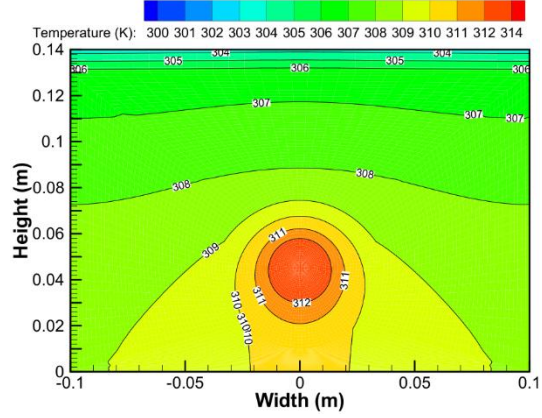
Table. 2. Properties of PCM and concrete as well as underfloor heating working conditions.

Parameters	Nomenclature	Value	Unit
Type of PCM	$[-]$	$\text{Na}_2\text{HPO}_4 \cdot 12\text{H}_2\text{O}$	$[-]$
Latent heat of PCM	ΔH_{PCM}	265	kJ/kg
Density of PCM	ρ_{PCM}	1507	kg/m^3
Temperature of transition of PCM	T_{mel}	37	$^\circ\text{C}$
Specific heat at constant pressure of PCM	C_{p-PCM}	1.69	$\text{kJ/kg} \cdot \text{K}$
Thermal conductivity of PCM	κ_{PCM}	0.514	$\text{W/m} \cdot \text{K}$
Thermal conductivity of copper coil	κ_C	397	$\text{W/m} \cdot \text{K}$
Type of concrete	$[-]$	C30	$[-]$
Specific heat at constant pressure of concrete	C_{p-conc}	0.97	$\text{kJ/kg} \cdot \text{K}$
Thermal conductivity of concrete	κ_{con}	1.6	$\text{W/m} \cdot \text{K}$
Density of concrete	ρ_{conc}	2300	kg/m^3
Thickness of the concrete	δ_{con}	0.13	m
Thickness of the wood floor	δ_{floor}	0.01	m
Volume flow rate of circulating water	V_{cw}	2.5	m^3/h

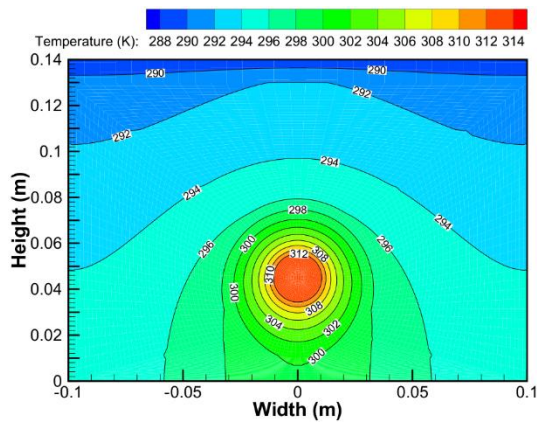
Fig. 8 (a~~~lc~~) presents the simulation results of heat transfer in build-in PCM heat storage unit at different time which carried out by software of Ansys Fluent 17.0. The thermal conductivity of the heat transfer between the coil and PCM has been considered in the setup of the boundary conditions. Thus, the boundary conditions of inner and outer tube have been set as “coupled” in Ansys Fluent 17.0 which means the solution of heat transfer process would be carried out through the coupled method in the program. The initial temperature of the heat storage unit is 15°C , and the underfloor heating can reach above 30°C after 39 hours when the circulating water is 40°C . As shown in Fig. 8(~~md~~), the floor temperature increases with time and reaches 25°C in the first 12 hours which has 10°C difference with the ambient. The changing curve mountains rapidly in the initial stage and becomes steady after 39 hours, the build-in PCM heat storage would supply heat to indoor area and maintain the room temperature.



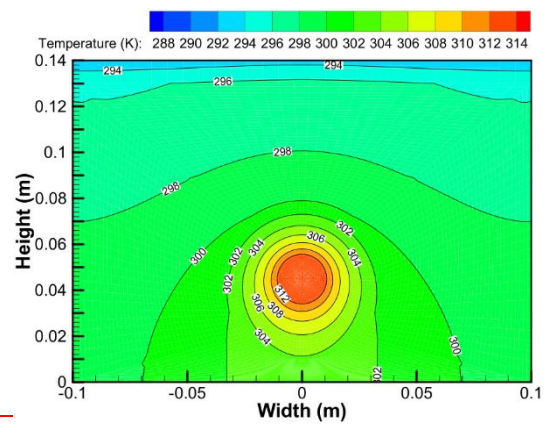
(a) Initial stage



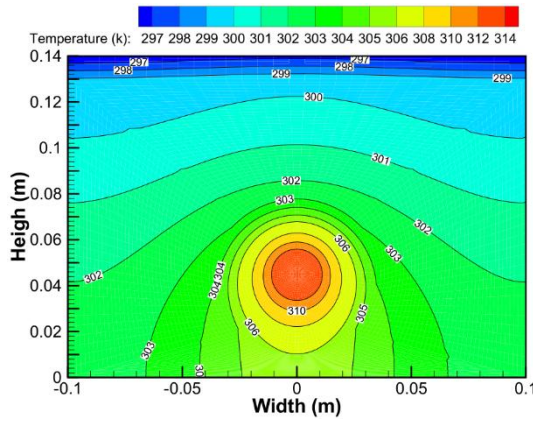
(b) Steady stage



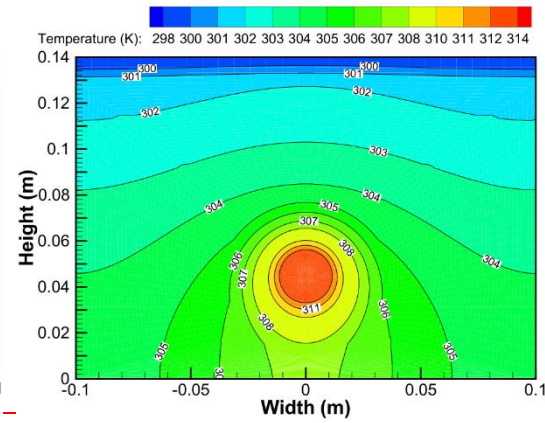
(c) 3 hours



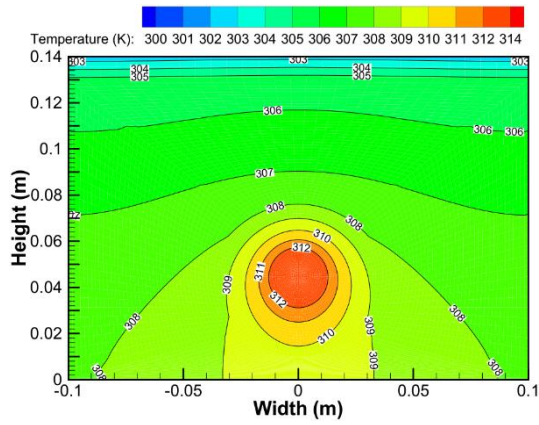
(d) 6 hours



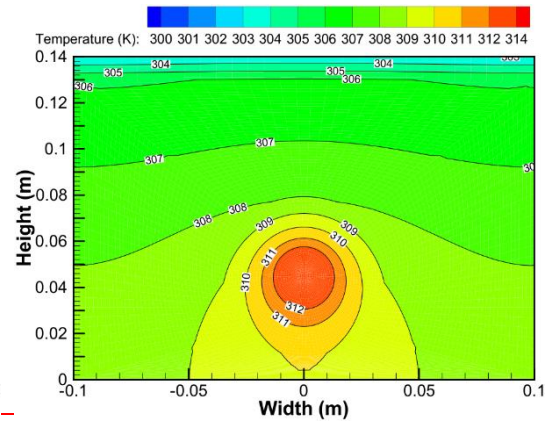
(e) 9 hours



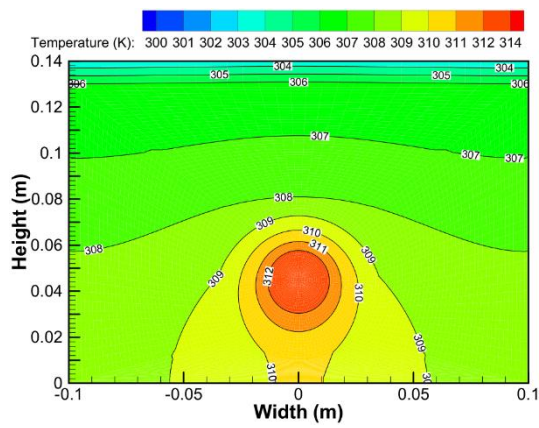
(f) 12 hours



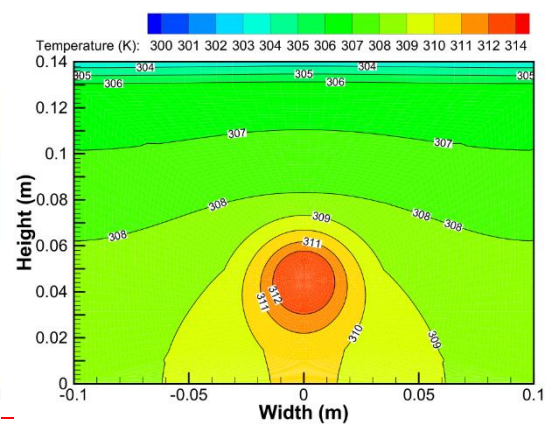
(g) 24 hours



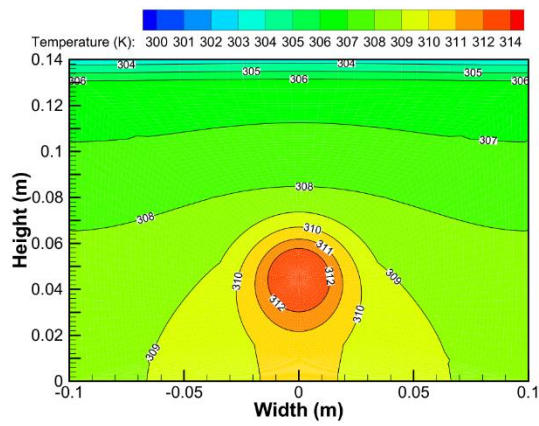
(h) 30 hours



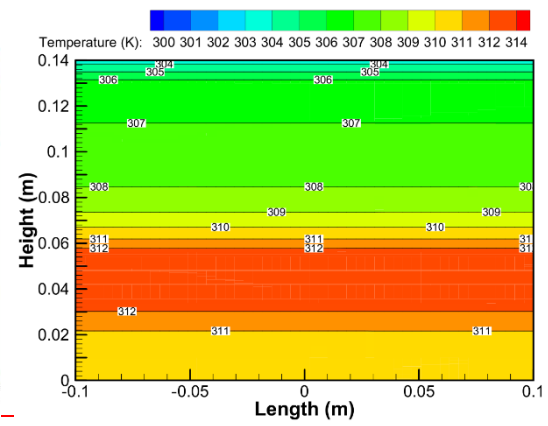
(i) 33 hours



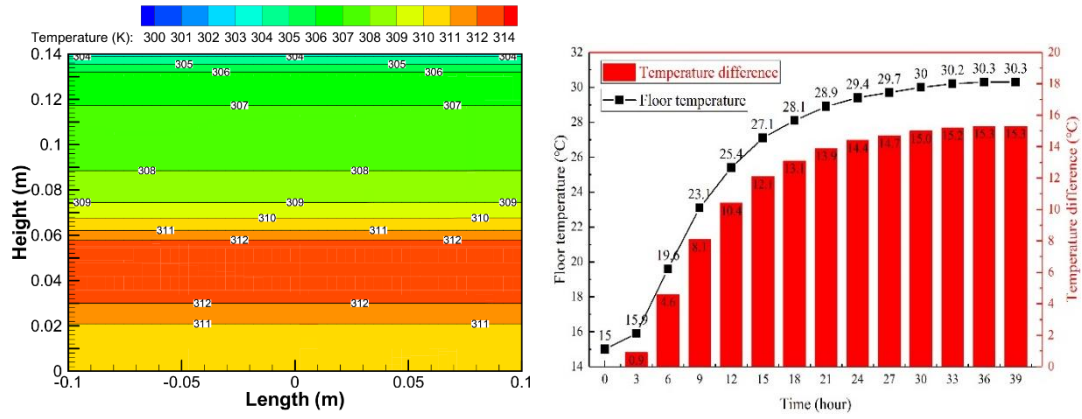
(j) 36 hours



(k) 39 hours



(l) Cross-section view at the width of 0 (39 hours)



(c) Cross-section view at the width of 0 (steady stage)

(d)

Fig. 8. (a-d) Cross-section temperature contour of the build-in PCM heat storage unit at different time. (m) Variation curve of floor temperature and temperature difference between floor and ambient.

Fig. 8. (a-c) Cross-section temperature contour of the build-in PCM heat storage unit at initial and steady stage. (d) Variation curve of floor temperature and temperature difference between floor and ambient.

Fig. 9 shows the variation curves of circulating water temperature and floor temperature with the length of circulating water tube. The temperature of circulating water would decrease from 40 °C (inlet) to 32.5 °C (outlet) while the floor temperature varies from 30.4 °C to 22.9 °C. This figure also presents the three temperature range of underfloor heating which can divided into three categories: Temperature range of no person staying area (29 °C-35 °C), Temperature range of short-time staying area (25 °C-29 °C) and Temperature range of long-time staying area (20 °C-25 °C). For a typical family, the heating area is about 100 m² which needs about 150 meters of underfloor heating tube (circulating water tube). As shown in Fig. 9, the first 30 meters tube can arrange in the no person staying area (storage room etc.) while 30 to 110 meters tube can arrange in the short time staying area (living room, kitchen etc.), and 110 to 150 meters tube can arrange in the long time staying area (bedroom etc.). Therefore, when using build-in PCM heat storage as underfloor heating, the system could meet the heat demand of users and keep indoor temperature steady.

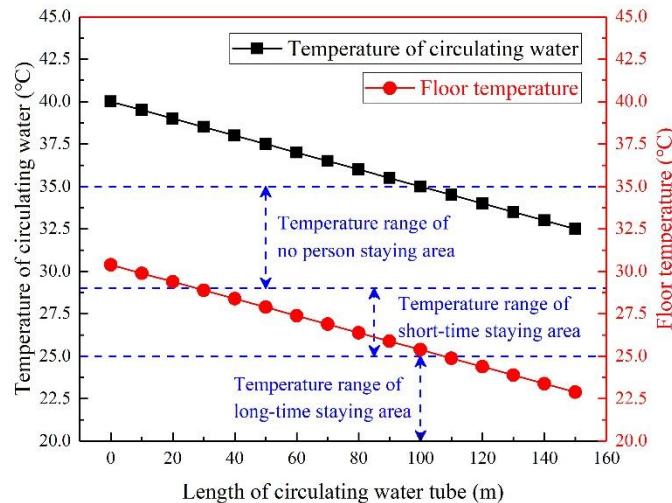


Fig. 9. Variation curves of circulating water temperature and floor temperature with the length of circulating water tube.

3.3. Model of compressor

The refrigerant mass flow rate \dot{m}_{ref} could be calculated by (Ma, 2013)

$$\dot{m}_{ref} = \lambda \cdot V_{th} / v_{suc} \quad (14)$$

where the λ is the compressor volumetric efficiency, V_{th} is the theoretical displacement volume of compressor (m^3), v_{suc} is the specific volume of the refrigerant in the suction period (m^3/kg).

The power consumption of compressor is written as:

$$P_{com} = \dot{m}_{ref} \cdot (h_{dis} - h_{suc}) / \eta_{ele} \quad (15)$$

where η_{ele} is the efficiency of the compressor which can be expressed by (Ma, 2013):

$$\eta_{ele} = -0.17938 + 0.87501 \frac{p_{dis}}{p_{suc}} - 0.30014 \left(\frac{p_{dis}}{p_{suc}} \right)^2 + 0.04135 \left(\frac{p_{dis}}{p_{suc}} \right)^3 - 0.00206 \left(\frac{p_{dis}}{p_{suc}} \right)^4 \quad (16)$$

The refrigerant vapor through compressor is isentropic, thus the equation can be expressed by:

$$T_{dis} / T_{suc} = (p_{dis} / p_{suc})^{(\chi-1)/\chi} \quad (17)$$

where the χ is the polytropic index of refrigerant. h_{dis} is the enthalpy of the vapor after compressed (kJ/kg), h_{suc} is the enthalpy of the vapor before compressed (kJ/kg).

The heat of refrigerant absorbed from the PV/T collector/evaporator equal to Q_u :

$$\dot{m}_{ref} \cdot (h_{eva,out} - h_{eva,in}) = Q_u = Q_{th} \quad (18)$$

3.4 Definition of the system performance

The COP (Coefficient of Performance) of the system can be defined as the ratio of overall heat output of system and power consumption of the compressor as following (R. Turns, 2006)

$$COP = \dot{m}_{ref} \cdot (h_{cond,in} - h_{cond,out}) / P_{com} \quad (19)$$

The η_{th} is the PV/T collector/evaporator's thermal efficiency, which can be defined as:

$$\eta_{th} = Q_{th} / (A \cdot I) \quad (20)$$

The η_e is the PV cells electrical efficiency which can be defined as:

$$\eta_e = Q_e / (A \cdot I) \quad (21)$$

The η_{ove} is the overall efficiency which can be defined as:

$$\eta_{ove} = (Q_{cond} + Q_e) / (A \cdot I) \quad (22)$$

3.5 Presentation of the algorithm by flow chart

The numerical simulation procedure of the system is shown in Fig. 10 to predict the system performance using the software of MATLAB. The solution steps are as flows:

- (1) Input all the environmental parameters, such as solar radiation intensity, wind speed, ambient temperature, etc.
- (2) Input the system design parameters and operation parameters, such as collector area, packing factor, collector slop, transmissivity of external glass cover, PV-glazing cover, thickness of each layer, etc.
- (3) Assume the temperature of PV cells T_p .
- (4) Calculate the overall heat loss rate Q_L , and the PV electrical output power Q_e .
- (5) Calculate the thermal energy gain rate through PV/T collector/evaporator Q_{th} , and the useful heat transfer rate by refrigerant Q_u .
- (6) Calculate $(Q_{th} - Q_u)/Q_{th}$. If $|(Q_{th} - Q_u)/Q_{th}| < 0.1\%$, the system achieves the heat balance and move to next step.
- (7) Input the superheat degree T_{sh} .
- (8) Assume the compressor discharge pressure P_{dis} .
- (9) Calculate the PV/T collector/evaporator inlet enthalpy $h_{eva,in}$ and the PCM heat exchanger outlet enthalpy $h_{cond,out}$. If $|(h_{eva,in} - h_{cond,out})/h_{cond,out}| < 0.1\%$, the system achieves the pressure balance and move to next step.
- (10) Calculate the COP, PCM melting rate \dot{m} , thermal efficiency η_{th} , electrical efficiency η_e , and overall efficiency η_{ove} .
- (11) Results output, and stop the program.

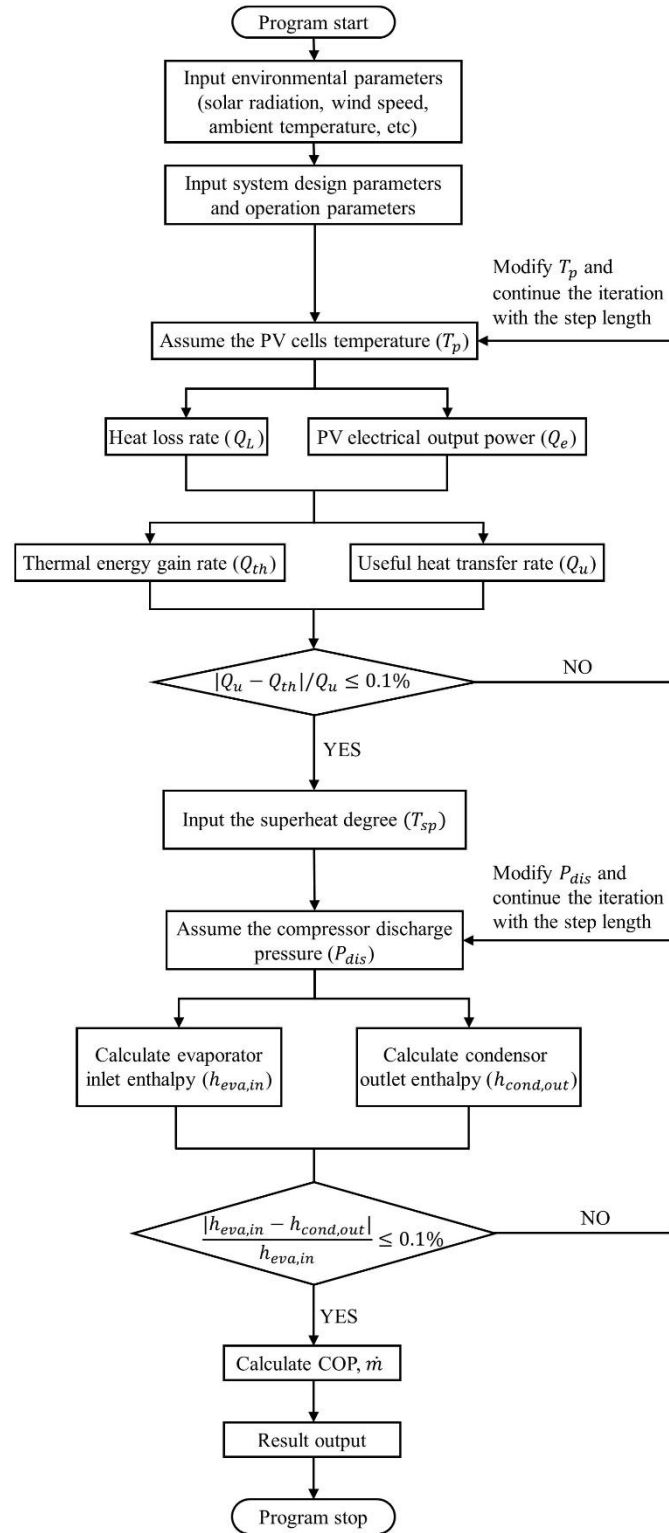


Fig. 10. Numerical solution procedure of the system.

4 Validation of the model

To ensure the reliability of the mathematic model, the simulation results should be compared with the experimental results. The experimental parameters used in the simulation are listed in Table. 3.

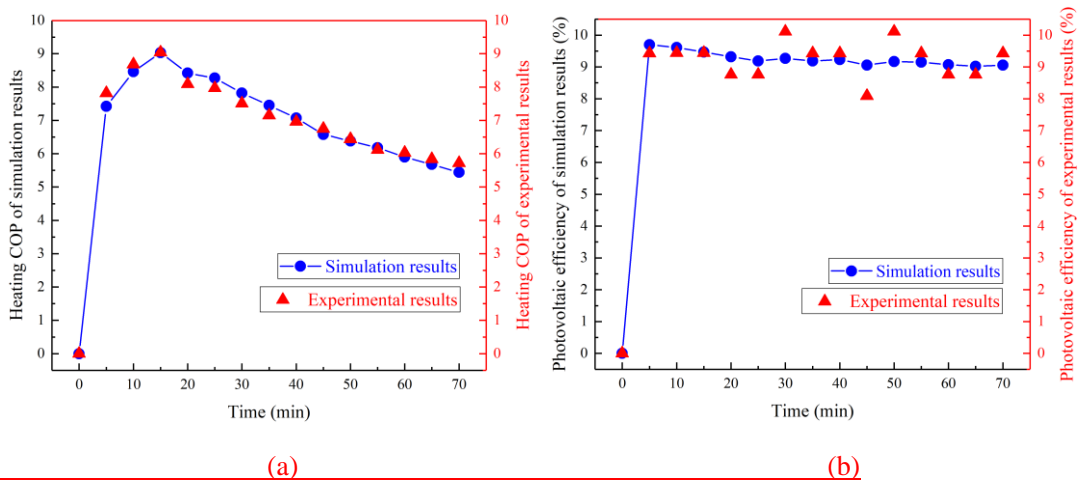
370

Table. 3. Experimental parameters (Zhou et al., 2019).

Parameters	Nomenclature	Value	Unit
Thickness of glass cover	δ_g	3.2	mm
Thickness of air gap	δ_{air}	35	mm
Thickness of PV-glazing cover	$\delta_{g,pv}$	1	mm
Thickness of PV cells	δ_{pv}	0.2	mm
Thickness of EVA adhesive film	δ_{EVA}	0.4	mm
Thickness of electrical insulation	δ_{ei}	0.5	mm
Length of PV/T	L	3.0	m
Width of PV/T	W	1.6	m
Wind speed	v_{wind}	1.5	m/s
Ambient temperature	T_a	298.5	K
Refrigerant type	ref	R22	[-]
Packing factor	β_p	0.64	[-]

371

372 The comparison results of heating COP are presented in Fig. 11(a), the operating conditions
373 are refer from Zhou et al.(Zhou et al., 2019). Under the same system components (PV/T
374 collector/evaporator, compressor, condenser, expansion valve, water tank), the simulation results
375 are in good agreement with the experimental results. Heating COP of the PV/T system increases in
376 the first 15 minutes because the water in the tank still in the low temperature range. Thus, the
377 temperature differences between the refrigerant fluid and water remains large in the condenser
378 leading to a high heat transfer efficiency. However, the heat transfer efficiency of the condenser
379 would be decreased when the temperature of the inlet water rises up during the operation of the
380 whole system. That is the reason of the reduction of heating COP after 15 minutes. The average
381 error of heating COP is 2.84% while the maximum error is 5.12%. Fig. 12-11(b) presents the
382 experimental and simulation results of the photovoltaic efficiency. The maximum photovoltaic
383 efficiency is 10.11% while the minimum is 8.09%, but all the experimental photovoltaic
384 efficiencies fluctuate around 9.24%. The simulation photovoltaic efficiencies remain around 9.25%
385 but fluctuate from 9.01% to 9.7% due to the influence of solar radiation intensity. The average
386 error of photovoltaic efficiency is 4.48% while the maximum error is 9.30%.



387

388

389 **Fig. 11. (a)** Comparison results of experimental and simulated heating COP. **(b)** Comparison
390 results of experimental and simulated photovoltaic efficiency.

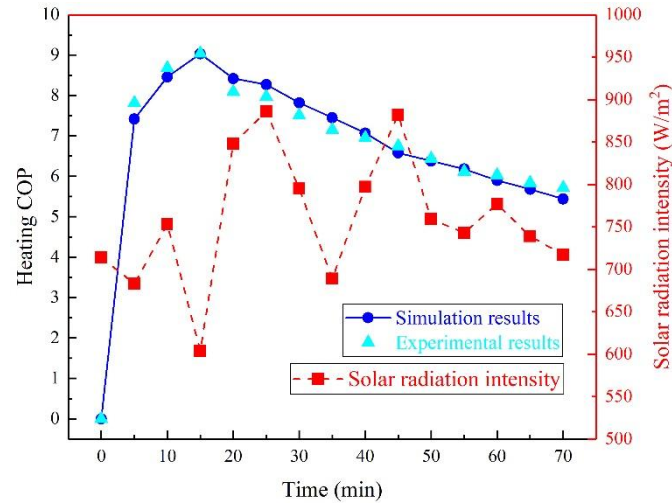


Fig. 11. Comparison results of experimental and simulated heating COP.

Fig. 12 presents the experimental and simulation results of the photovoltaic efficiency. The maximum photovoltaic efficiency is 10.11% while the minimum is 8.09%, but all the experimental photovoltaic efficiencies fluctuate around 9.24%. The simulation photovoltaic efficiencies remain around 9.25% but fluctuate from 9.01% to 9.7% due to the influence of solar radiation intensity. The average error of photovoltaic efficiency is 4.48% while the maximum error is 9.30%.

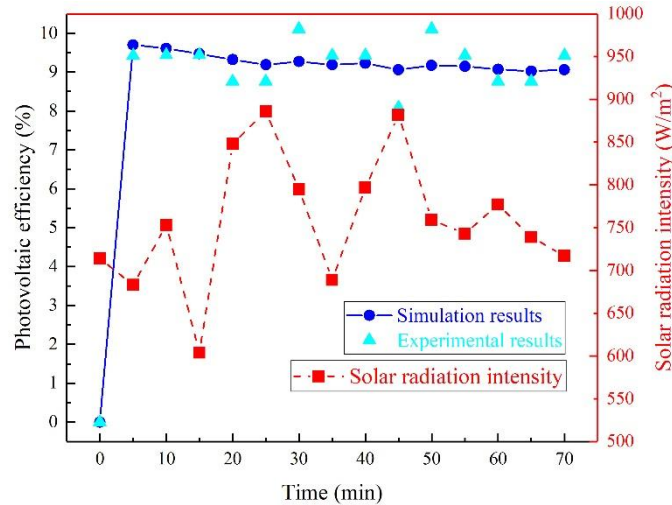


Fig. 12. Comparison results of experimental and simulated photovoltaic efficiency.

5 Parameter analysis

In this section, the influences of different parameters (solar radiation intensity, ambient temperature, wind speed, area of PV/T collector) on this system are investigated, and the performance indices of the system under typical working conditions are also given. It should be noted that when one parameter is varied, others keep constant. Pressure ratio of the compressor refers the ratio of pressure of discharged refrigerant vapor and charged refrigerant vapor.

5.1 Solar radiation intensity

The influences of solar radiation intensity which varying from 200 W/m² to 1000 W/m² are shown as follows at the working conditions are: ambient temperature is 25 °C, wind speed is 1.5 m/s and area of PV/T collector is 2 m².

Fig. 12 presents the rising curve of the heating COP and declining curves of thermal, electrical and overall efficiencies. The heating COP is 3.0 for a solar radiation of 200 W/m², and it can reach up to 10.8 when the solar radiation is 1000 W/m². The refrigerant evaporation temperature and pressure will be increased due to a higher temperature of PV cells. Thus, the compressor consumes less electricity to compress the refrigerant vapor leading to this upward trend. Meanwhile, the heat loss will mount due to a higher temperature difference between PV cells and ambient. Thereby, the thermal and electrical efficiencies of the PV/T panel reduce resulting in a reduction of the overall efficiency.

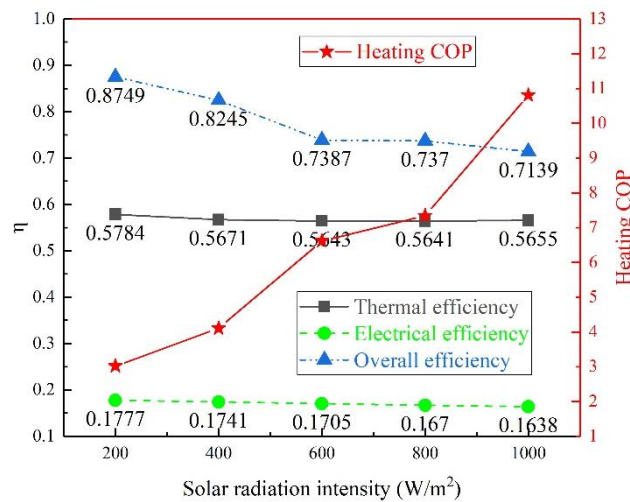


Fig. 12. Influence of solar radiation intensity on heating COP and thermal, electrical, overall efficiencies.

Fig. 13 shows the effect of solar radiation intensity on thermal and electrical output power, pressure ratio and mass flow rate of refrigerant. The thermal and electrical power keep mounting with the increase of the solar radiation intensity. Meanwhile, the pressure ratio of the compressor decreases and the mass flow rate of the refrigerant increases. That is because the increase of the evaporation temperature causes a higher evaporation pressure which equals to the suction pressure of compressor leading to a lower pressure ratio. Furthermore, a larger amount of refrigerant will be needed to transfer extra heat from PV/T collector/evaporator to PCM heat exchanger (condenser) when the PV/T panel absorbs more heat from solar radiation.

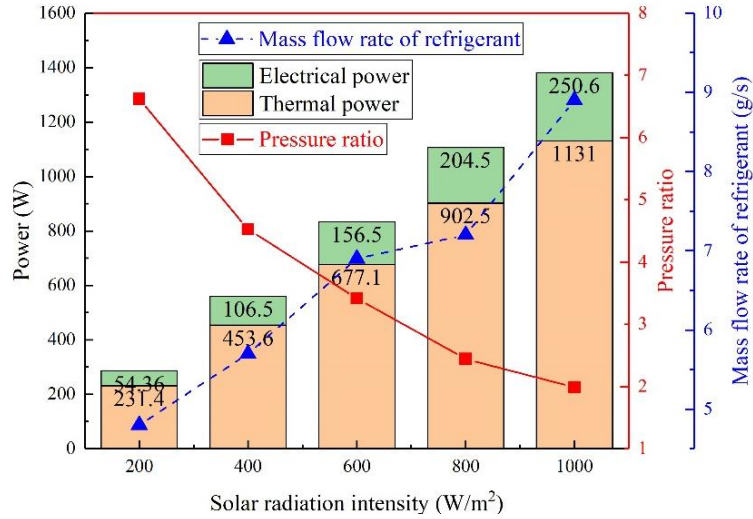


Fig. 13. Influence of solar radiation intensity on electrical and thermal power, pressure ratio and mass flow rate of refrigerant.

As shown in Fig. 14, there is a positive linear correlation between PV cells' electrical power generation and solar radiation intensity while the consumption power of compressor fluctuates around 120 W. When the output power to grid is less than zero, it means the system consumes electricity from the power grid. The electrical power generated by PV panels could meet the demand of the compressor and the system could output electricity to power grid when the solar radiation intensity exceeds 500 W/m².

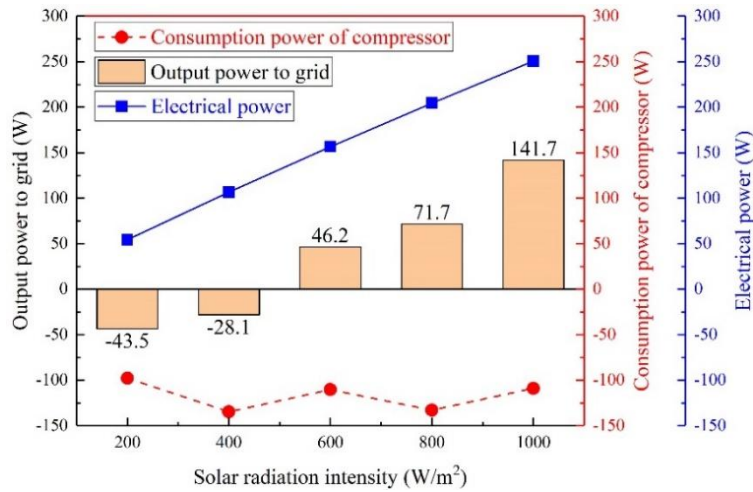


Fig. 14. Influence of solar radiation intensity on electrical power, consumption power of compressor and output power to grid.

5.2 Ambient temperature

The influences of ambient temperature which varying from 15 °C to 35 °C are shown as follows at the working conditions are: solar radiation intensity is 600 W/m², wind speed is 1.5 m/s and area of PV/T collector is 2 m².

Fig. 15 shows that increasing the ambient temperature will increase the heating COP and thermal efficiency but decrease the electrical and overall efficiencies. The temperature difference between PV cells and ambient will reduce when the ambient temperature rises leading to a less

heat loss from PV/T panel to the surrounding. Thus, the heating COP increases and the electrical efficiency decreases due to a higher temperature of the PV cells while the thermal efficiency increases. However, the electrical efficiency outweighs the thermal efficiency resulting in a reduction of the overall efficiency when the ambient temperature is below 25 °C. The heating COP (9.25) at 35 °C is higher than COP (5.79) at 15 °C by 59.8%, thus a higher ambient temperature is better for the system performance.

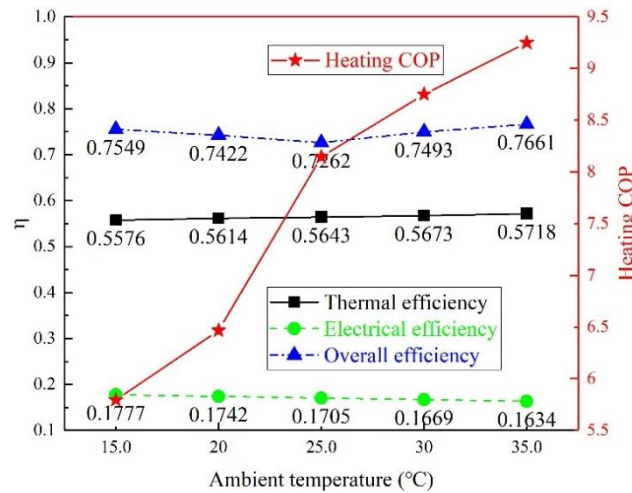


Fig. 15. Influence of ambient temperature on heating COP and thermal, electrical, overall efficiencies.

The variation curves of thermal and electrical power, pressure ratio and mass flow rate of refrigerant with the increase of ambient temperature are shown in Fig. 16. The changing curves of the electrical and thermal output power are the same as the electrical and thermal efficiencies. The pressure ratio of the compressor will increase when the ambient temperature is below 25 °C and decrease when the ambient temperature is over 25 °C. That is because a lower ambient temperature leads to a lower superheat degree of refrigerant which cause a lower pressure ratio, and in the opposite, a higher ambient temperature leads to a higher superheat degree. Moreover, when the ambient temperature exceeds 25 °C, it will influence the thermal efficiency of PV/T collector causing the reduction of pressure ratio. The mass flow rate of the refrigerant will keep climbing when the ambient temperature rises because less heat will lose in the ambient while more heat will be absorbed by refrigerant.

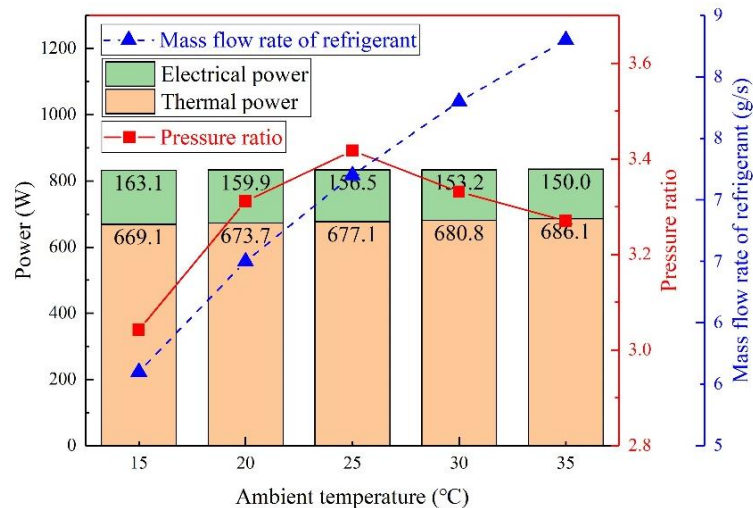


Fig. 16. Influence of ambient temperature on electrical and thermal power, pressure ratio and mass flow rate of refrigerant.

As shown in Fig. 17, the electrical power of PV decreases linearly with the ambient temperature while the consumption power of compressor decreases when the ambient temperature is below 25 °C and increases when the ambient temperature exceeds 25 °C. The output power to grid reaches its maximum at 25 °C. Because when the ambient temperature is below 25 °C, the effect of environmental heat loss is greater than that of heat-collecting efficiency due to a large temperature difference. However, the effect of a higher ambient temperature on heat-collecting efficiency is greater than that of environmental heat loss when the ambient temperature exceeds 25 °C.

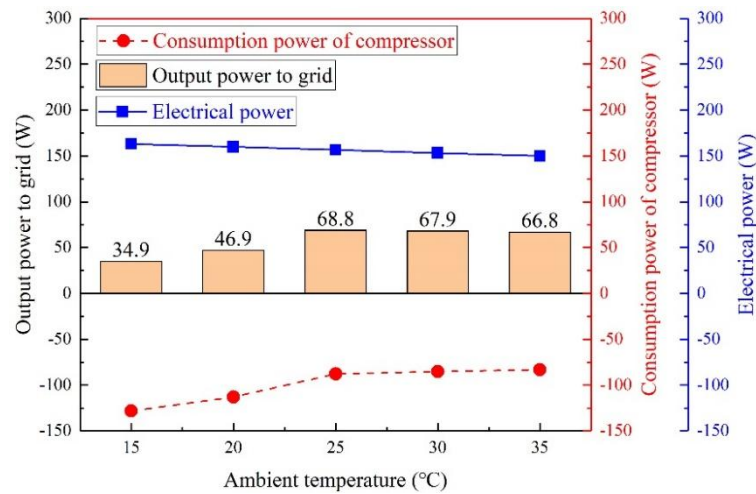


Fig. 17. Influence of ambient temperature on electrical power, consumption power of compressor and output power to grid.

5.3 Wind speed

The influences of wind speed which varying from 0.5 m/s to 2.5 m/s are shown as follows at the working conditions are: solar radiation intensity is 600 W/m², ambient temperature is 25 °C and area of PV/T collector is 2 m².

Fig. 18 shows the variation curve of heating COP, thermal, electrical and overall efficiencies with wind speed varying from 0.5 m/s to 2.5 m/s. The heating COP will decrease rapidly when the wind speed is low and steadily when the wind speed increases. More heat will be transferred to the environment and less heat is absorbed by the PV/T panel under a higher wind speed. Meanwhile, evaporation temperature of refrigerant will be decreased and the consumption power of compressor will be increased when the temperature of PV cells rises. Thus, the heating COP drops from 9.4 to 6.8, which means better wind protection measures should be taken to improve the system performance.

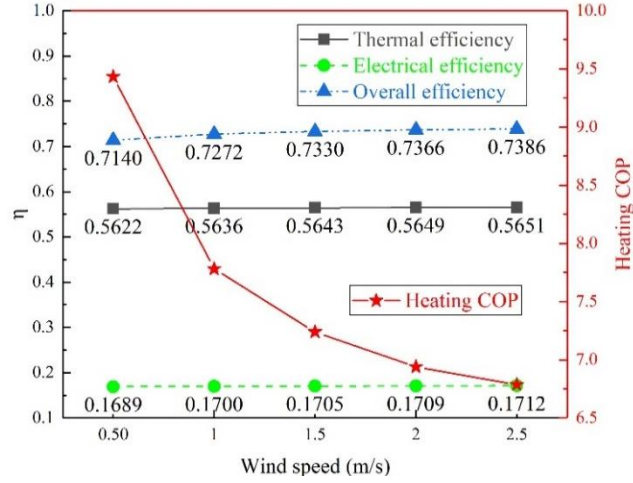


Fig. 18. Influence of wind speed on heating COP and thermal, electrical, overall efficiencies.

The variation curves of thermal and electrical power, pressure ratio and mass flow rate of the refrigerant with the increase of wind speed are shown in Fig. 19. The changing curves of the thermal and electrical power have the same trend as the thermal and electrical efficiencies. Both the pressure ratio and mass flow rate of refrigerant reduce with the increase of the wind speed. That is because more heat will be absorbed by the ambient air while less heat will be transferred by the refrigerant.

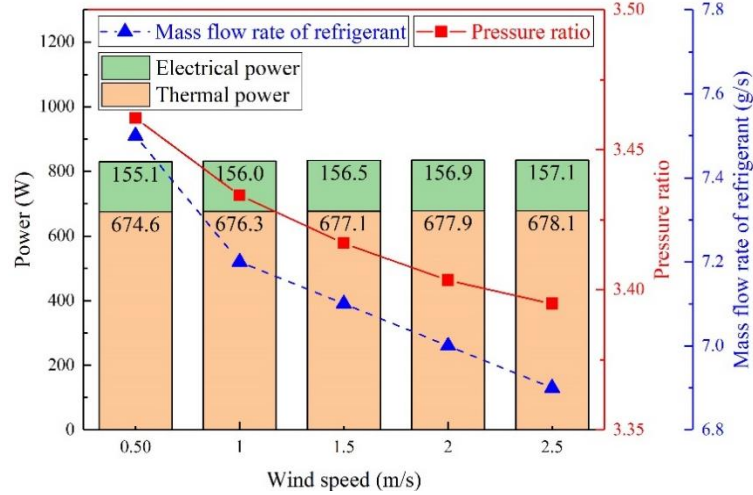


Fig. 19. Influence of wind speed on electrical and thermal power, pressure ratio and mass flow rate of refrigerant.

Fig. 20 presents the influence of wind speed on electrical power, consumption power of compressor and output power to grid. The output power to grid decreases rapidly when the wind speed increases from 0.5 m/s to 1.5 m/s and steadily when the wind speed exceeds 1.5 m/s. More heat will loss in the environment due to a higher wind speed, and the thermal efficiency will decrease causing a higher consumption power of compressor.

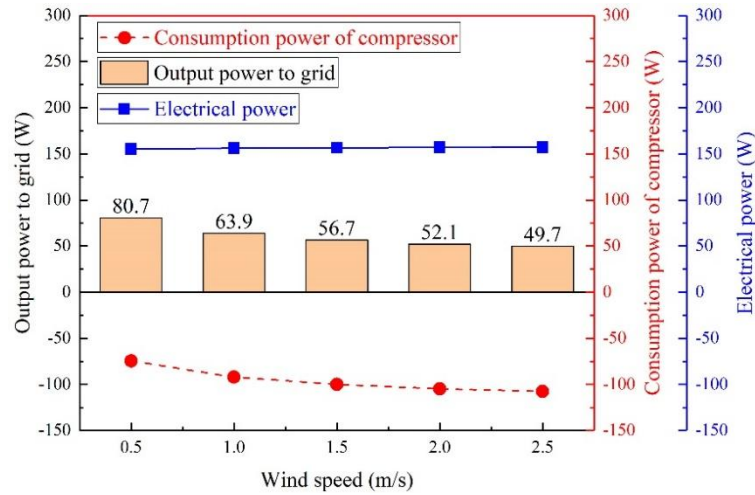


Fig. 20. Influence of wind speed on electrical power, consumption power of compressor and output power to grid.

5.4 Area of PV/T collector

The influences of the area of PV/T collector which varying from 1 m² to 3 m² are shown as follows at the working conditions are: solar radiation intensity is 600 W/m², ambient temperature is 25 °C and wind speed is 1.5 m/s.

Fig. 21 presents the influence of the area of PV/T collector on pressure ratio, heating COP and overall efficiency. Pressure ratio and overall efficiency reduce with the increase of the area, while the heating COP mounts. That is because a larger area can absorb more heat from the solar radiation, and the extra heat will be transferred by PV/T panel to refrigerant. Meanwhile, the evaporation temperature and pressure will increase leading to a lower pressure ratio and a higher heating COP. The consumption power of the compressor will decrease when the pressure ratio reduces, thus the heating COP increases more rapidly under large area conditions. A higher temperature of the PV cells causes more heat dissipates in the ambient resulting a decrease of the overall efficiency.

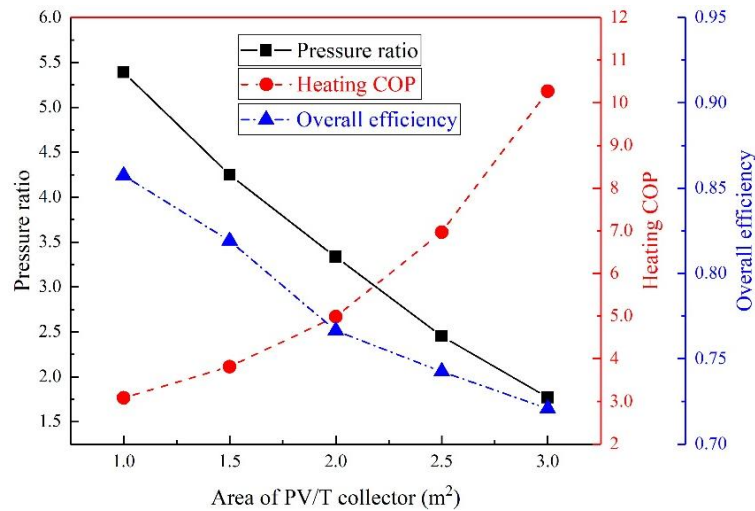


Fig. 21. Influence of the area of PV/T collector on pressure ratio, heating COP and overall efficiency.

Fig. 22 shows the declining trends of the pressure ratio and increasing trends of the thermal and electrical power influenced by the area of PV/T collector. The thermal and electrical output power are almost linearly and positively correlated with the area of PV/T collector. That is because more heat will gain from the solar radiation and be transferred to the refrigerant when the area increases.

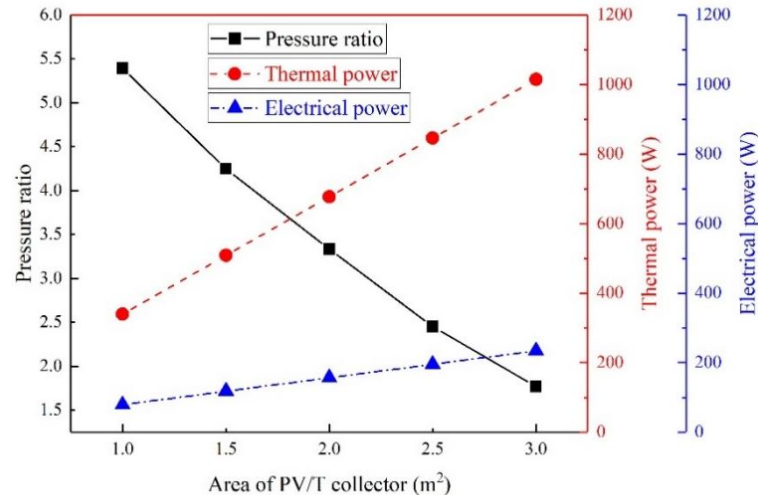


Fig. 22. Influence of the area of PV/T collector on pressure ratio, thermal and electrical power.

As shown in Fig. 23, the mass flow rate of refrigerant will increase when the area increases, while the consumption power of compressor will increase when the area is below 1.5 m² and decrease when the area is over 1.5 m². The mass flow rate of refrigerant will increase because the latent heat and heat capacity of refrigerant are the same when more heat is transferred to the refrigerant. The heat absorbed by the PV/T panel and mass flow rate of refrigerant are low, thus the compressor consumes less electricity to compress the refrigerant vapor. With the increase of the area, the mass flow rate mounts resulting in an increase of consumption power. However, the pressure ratio of the compressor will reduce when the area increases over 1.5 m² leading to a lower consumption power.

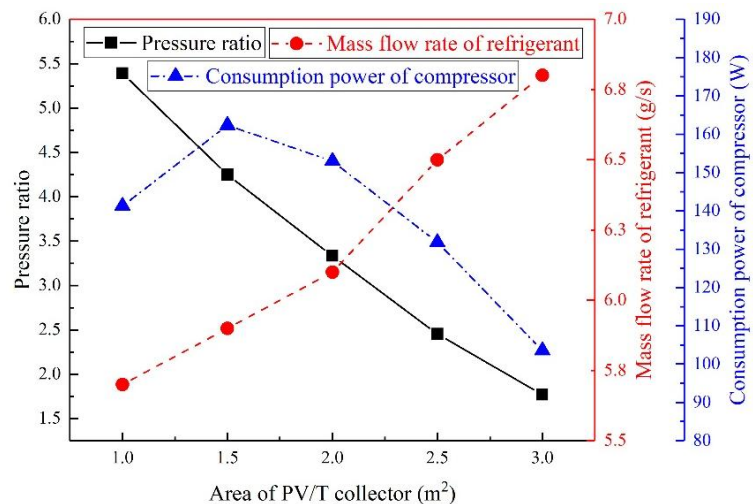


Fig. 23. Influence of the area of PV/T collector on pressure ratio, mass flow rate of refrigerant and consumption power of compressor.

Fig. 24 illustrates the variation curve of output power to grid with the area of PV/T collector. The electrical power generated by PV panels will meet the demand of compressor when the area of PV/T collector is 2 m^2 . Moreover, the PV cells start to produce electricity to power grid when the area is over 2 m^2 which means a larger PV/T panel is better for the system performance under the same system conditions.

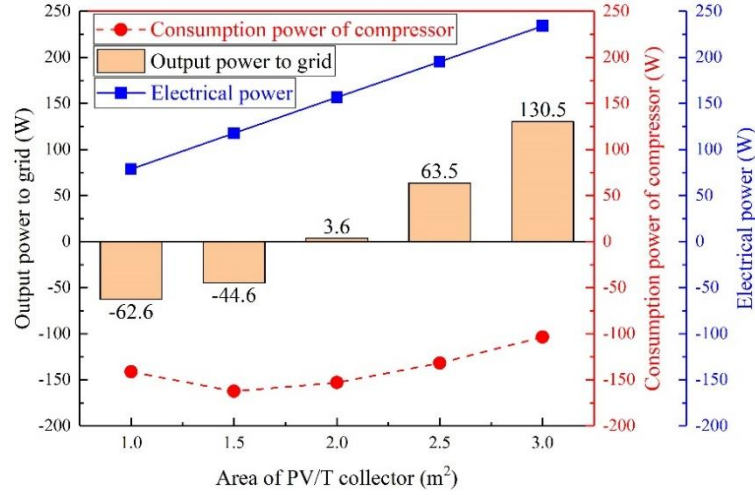


Fig. 24. Influence of area of PV/T collector on electrical power, consumption power of compressor and output power to grid.

5.5 Feasibility analysis of the system

Nowadays, the Chinese government promotes the policy of using electricity for residential heating instead of burning coal for heating in northern China to reduce carbon dioxide emissions. The solar PV/T heat pump coupled with build-in PCM heat storage system is suitable for residential heating due to its advantages: (1) high efficiency; (2) low energy consumption; (3) stable residential heating supply; (4) zero carbon emissions. Table. 4 presents the typical operating conditions and parameters of the system. It is a typical spring/autumn day in northern China.

Table. 4. Typical operating conditions and parameters of the system.

Parameters	Nomenclature	Value	Unit
Solar radiation intensity	I	600	W/m^2
Sunshine duration	t_s	8	hour
Ambient temperature	T_a	15	$^{\circ}\text{C}$
Wind speed	v_{wind}	1.5	m/s
Area of the collector	A	20	m^2
Packing factor	β_p	1	[-]
Heating area	A_{ha}	100	m^2
Heat loss per square meter	P_L	50	W/m^2
Filling volume of the PCM	V_{PCM}	0.57	m^3
External diameter of the inside pipe	D_1	0.012	m
Internal diameter of the inside pipe	d_1	0.010	m
External diameter of the outside pipe	D_2	0.074	m
Internal diameter of the outside pipe	d_2	0.072	m

Table. 5 presents the simulation performance indices of the system under typical day conditions. The PV/T collector can transfer 213.9 MJ heat from the ambient to the PCM heat exchanger, and the heat will be stored in phase change materials and concrete. The build-in PCM heat storage can release the heat for 10 hours at 5.94 kW during the night while the heat loss power of 100 m² area is 5 kW. During autumn, winter and early spring in northern China, the heating system is necessary to keep indoor temperature above 20°C. Thus, the system can achieve the heating needs of the users and keep the indoor temperature steady. Meanwhile, the system can output 21.4% (2.79 kWh) of the power generated by PV panels to the grid while 78.6% of it consumed by the compressor. The heating COP of the system is 5.79, and the overall efficiency is 75.49%.

Table. 5. Simulation performance indices of the system under typical day conditions.

Parameters	Value	Unit
Total heat storage	213.9	MJ
Photovoltaic power	1.63	kW
Photovoltaic efficiency	17.77	%
PV/T thermal efficiency	55.76	%
Heating COP	5.79	[-]
Overall efficiency	75.49	%
Cumulative power generation	13.05	kWh
Consumption power of compressor	10.26	kWh
Output power to grid	2.79	kWh
Temperature range of underfloor heating	22-31	°C
Heating power at night	5.94	kW
Heat loss power	5.00	kW
Heating hour	10.00	hour

Table. 6 illustrates the comparison of cost between the proposed system and conventional air conditioning system. The operating cost of the proposed system is under zero because users could sell spare electricity to power grid and get profit. Fig. 25 shows the cost variation curves of these two systems. The initial cost of the proposed system is much higher than conventional air conditioning system due to the underfloor heating equipment and PV/T panels, etc. However, the air conditioning system consumes a lot of electricity during the night for heating supply. Thus, the cost of these two systems will be the same after about 4 years, and the cost of proposed system keeps reduce while the cost of air conditioning system still climbs. Moreover, underfloor heating system which using radiative heating is more comfort and silence for users than air conditioner.

Table. 6. Cost comparison between the proposed system and conventional air conditioning system.

Heating system	Initial cost (¥)	Operating cost (¥/year)	Maintenance cost (¥/year)
Proposed system	22000	-764	550
Air conditioning system	4500	4024	225

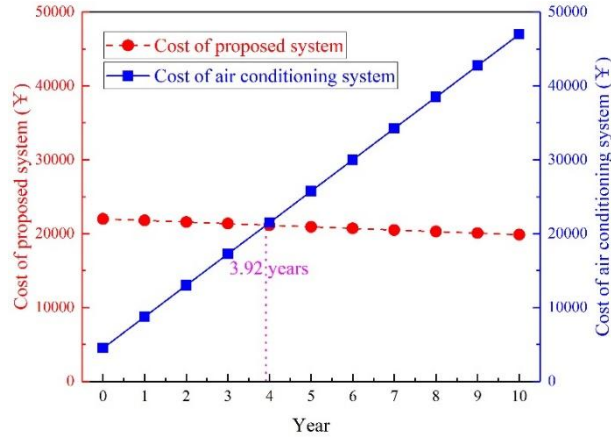


Fig. 25. Cost variation curves of proposed system and air conditioning system.

Moreover, Fig. 26 illustrates the comparison of thermal and electrical efficiencies of different PV/T systems. The electrical and thermal efficiencies of solar PV/T heat pump which proposed in this paper are higher than that of most air, water or PCM based PV/T systems. Thus, the solar PV/T heat pump coupled with build-in PCM heat storage system has a higher comprehensive energy utilization efficiency than most PV/T systems. Meanwhile, the adoption of PCM heat storage can also enhance the stability of solar PV/T heat pump system.

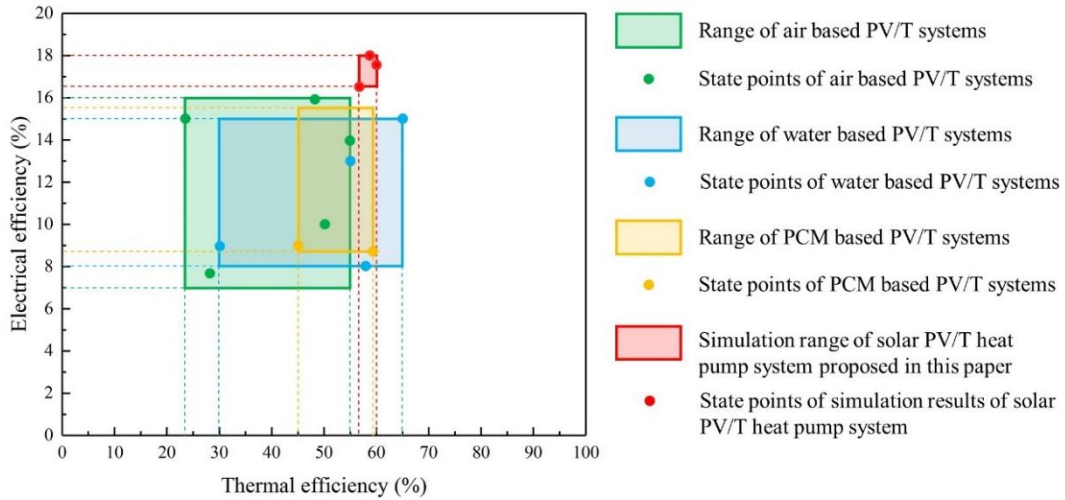


Fig. 26. Comparison of thermal and electrical efficiencies of different PV/T systems (Ahn et al., 2015; Al Waeli et al., 2017; Hu et al., 2016; Li et al., 2015; Mojumder et al., 2016; Qiu et al., 2015)

6 Conclusion

A building-coupled cogeneration system using solar PV/T heat pump and build-in PCM heat storage is proposed in this paper. The mathematical model of the system is established and verified to analyze the system performance under different conditions. The main conclusions can be drawn as follows:

(1) The temperature of underfloor heating which using build-in PCM heat storage can reach 22 °C to 31 °C after 39 hours when the circulating water is 40 °C which is stable and suitable for residential heating.

(2) The heating COP increases with the increase of solar radiation, ambient temperature, area

~~of PV/T collector, and decrease of wind speed, respectively. Solar radiation intensity and area of PV/T collector are two major factors affecting system performance compared to wind speed and ambient temperature.~~

(32) The heating COP can reach 6.6 which is 94% higher than conventional air conditioning system when solar radiation intensity is 600 W/m^2 , ambient temperature is 25°C , wind speed is 1.5 m/s and area of PV/T collector is 2 m^2 while the electrical, thermal and overall efficiencies are 17.05%, 56.43% and 73.87%, respectively.

(43) A 2 m^2 PV/T panel can meet the power demand of the system and heating demand of a 10 m^2 room when the solar radiation intensity is 500 W/m^2 . Moreover, the PV/T panel can output electricity to power grid if the panel area is bigger than 2 m^2 or solar radiation intensity is higher than 500 W/m^2 .

The mathematical model established in this paper can also be used to analyze and optimize the solar PV/T heat pump system. However, the mathematical model of this system is for stable working conditions instead of transient. The establishment of dynamic model is needed for further predict and analyze accurately of solar assisted heat pump system under dynamic working conditions.

Acknowledgements

This research work is funded by the International Research Cooperation Program of Shanghai (Grant No. 18160710500).

Nomenclature:

Symbols

A	area (m^2)
W	width of the PV/T collector/evaporator (m)
L	length of the PV/T collector/evaporator (m)
ΔH	latent heat (kJ/kg)
h	heat transfer coefficient ($\text{W/m}^2\cdot\text{K}$)
U	heat loss coefficient ($\text{W/m}^2\cdot\text{K}$)
C_p	specific heat at constant pressure ($\text{kJ/kg}\cdot\text{K}$)
d	inner diameter (m)
D	external diameter (m)
t/T	temperature (K)
I	solar radiation intensity (W/m^2)
Q	heat transfer rate (W)
F	collector efficiency (-)
R	thermal resistance ($\text{m}^2\cdot\text{K/W}$)
Re	Reynolds number (-)
Ra	Rayleigh number (-)
Pr	Prandtl number (-)

	v	wind speed (m/s)
	m	mass flowrate (kg/s)
	g	gravitational acceleration (m/s ²)
	p	pressure (kPa)
	P	power (W)
	V	volume flow rate (m ³ /h)
647		
648	Greek symbols	
	δ	thickness (m)
	τ	transmittance (-)
	a	absorption ratios (-)
	β	packing factor (-)
	ε	emissivity (-)
	κ	thermal conductivity (W/m·K)
	σ	Stefan-Boltzmann constant (-)
	ρ	density (kg/m ³)
	λ	compressor volumetric efficiency (-)
	η	efficiency (-)
	χ	polytropic index (-)
649		
650	Subscripts	
	p, pv	PV cells
	g, c_1	external glass cover
	c/c_2	PV-glazing cover
	$conc$	concrete
	EVA	EVA grease
	PCM	phase change material
	mel	melting point
	ref	refrigerant
	b	baseboard
	cv	convection
	rd	radiation
	rb	roll-bond panel pipe
	a	ambient
	l	liquid
	L	lost
	rc	reference
	e	electrical
	ei	electrical insulation
	u	uesful
	th/R	thermal
	tp	two-phase flow
	ove	oveall
	abs	absorb

<i>hp</i>	heat pipe
<i>sh</i>	superheated
<i>v</i>	vapor
<i>cond</i>	condensation
<i>eva</i>	evaporation
<i>ot</i>	outer pipe
<i>eq</i>	equivalent
<i>hx</i>	heat exchanger
<i>dis</i>	discharge
<i>suc</i>	suction
<i>in</i>	inlet
<i>out</i>	outlet
<i>cw</i>	circulating water

651

652 **References:**

- 653 2019. Review and outlook of world energy development, Non-Fossil Energy Development in China.
654 pp. 1-36.
- 655 Ahn, J.-G., Kim, J.-H., Kim, J.-T., 2015. A Study on Experimental Performance of Air-Type PV/T
656 Collector with HRV. Energy Procedia 78, 3007-3012.
- 657 Al-Waeli, A.H.A., Sopian, K., Kazem, H.A., Chaichan, M.T., 2017. Photovoltaic/Thermal (PV/T)
658 systems: Status and future prospects. Renewable and Sustainable Energy Reviews 77, 109-130.
- 659 Cabeza, L.F., Castell, A., Barreneche, C., de Gracia, A., Fernández, A.I., 2011. Materials used as
660 PCM in thermal energy storage in buildings: A review. Renewable and Sustainable Energy Reviews
661 15(3), 1675-1695.
- 662 Caetano, N.S., Mata, T.M., Martins, A.A., Felgueiras, M.C., 2017. New Trends in Energy
663 Production and Utilization. Energy Procedia 107, 7-14.
- 664 Del Amo, A., Martínez-Gracia, A., Bayod-Rújula, A.A., Cañada, M., 2019. Performance analysis
665 and experimental validation of a solar-assisted heat pump fed by photovoltaic-thermal collectors.
666 Energy 169, 1214-1223.
- 667 Diallo, T.M.O., Yu, M., Zhou, J., Zhao, X., Shittu, S., Li, G., Ji, J., Hardy, D., 2019. Energy
668 performance analysis of a novel solar PVT loop heat pipe employing a microchannel heat pipe
669 evaporator and a PCM triple heat exchanger. Energy 167, 866-888.
- 670 Fayaz, H., Rahim, N.A., Hasanuzzaman, M., Rivai, A., Nasrin, R., 2019. Numerical and outdoor
671 real time experimental investigation of performance of PCM based PVT system. Solar Energy 179,
672 135-150.
- 673 Fiorentini, M., Cooper, P., Ma, Z., Robinson, D.A., 2015. Hybrid Model Predictive Control of a
674 Residential HVAC System with PVT Energy Generation and PCM Thermal Storage. Energy
675 Procedia 83, 21-30.
- 676 Hosseinzadeh, M., Sardarabadi, M., Passandideh-Fard, M., 2018. Energy and exergy analysis of
677 nanofluid based photovoltaic thermal system integrated with phase change material. Energy 147,
678 636-647.
- 679 Hu, J., Chen, W., Yang, D., Zhao, B., Song, H., Ge, B., 2016. Energy performance of ETFE cushion
680 roof integrated photovoltaic/thermal system on hot and cold days. Applied Energy 173, 40-51.

Huang, B.J., Lee, C.P., 2004. Long-term performance of solar-assisted heat pump water heater. *Renewable Energy* 29(4), 633-639.

Huide, F., Xuxin, Z., Lei, M., Tao, Z., Qixing, W., Hongyuan, S., 2017. A comparative study on three types of solar utilization technologies for buildings: Photovoltaic, solar thermal and hybrid photovoltaic/thermal systems. *Energy Conversion and Management* 140, 1-13.

Jankowski, N.R., McCluskey, F.P., 2014. A review of phase change materials for vehicle component thermal buffering. *Applied Energy* 113, 1525-1561.

Kazemian, A., Salari, A., Hakkaki-Fard, A., Ma, T., 2019. Numerical investigation and parametric analysis of a photovoltaic thermal system integrated with phase change material. *Applied Energy* 238, 734-746.

Keček, D., Mikulić, D., Lovrinčević, Ž., 2019. Deployment of renewable energy: Economic effects on the Croatian economy. *Energy Policy* 126, 402-410.

Kuik, O., Branger, F., Quirion, P., 2019. Competitive advantage in the renewable energy industry: Evidence from a gravity model. *Renewable Energy* 131, 472-481.

Kuznik, F., Virgone, J., Roux, J.-J., 2008. Energetic efficiency of room wall containing PCM wallboard: A full-scale experimental investigation. *Energy and Buildings* 40(2), 148-156.

Li, G., Pei, G., Ji, J., Yang, M., Su, Y., Xu, N., 2015. Numerical and experimental study on a PV/T system with static miniature solar concentrator. *Solar Energy* 120, 565-574.

Ma, Y., 2013. Analysis of Electrical Efficiency for Positive Displacement Refrigerant Compressor. *Journal of Refrigeration*.

Mojumder, J.C., Chong, W.T., Ong, H.C., Leong, K.Y., Abdullah Al, M., 2016. An experimental investigation on performance analysis of air type photovoltaic thermal collector system integrated with cooling fins design. *Energy and Buildings* 130, 272-285.

Nahar, A., Hasanuzzaman, M., Rahim, N.A., 2017. A Three-Dimensional Comprehensive Numerical Investigation of Different Operating Parameters on the Performance of a Photovoltaic Thermal System With Pancake Collector. *Journal of Solar Energy Engineering* 139(3), 031009.

Othman, M.Y., Hamid, S.A., Tabook, M.A.S., Sopian, K., Roslan, M.H., Ibarahim, Z., 2016. Performance analysis of PV/T Combi with water and air heating system: An experimental study. *Renewable Energy* 86, 716-722.

P. Hartnett, J., M. Rohsenow, W., 1973. *Handbook of Heat Transfer*.

Paolo Frankl, S., 2010. *Technology Roadmap: Solar Photovoltaic Energy*.

Pereira da Cunha, J., Eames, P., 2016. Thermal energy storage for low and medium temperature applications using phase change materials – A review. *Applied Energy* 177, 227-238.

Pietrosemoli, L., Rodríguez-Monroy, C., 2019. The Venezuelan energy crisis: Renewable energies in the transition towards sustainability. *Renewable and Sustainable Energy Reviews* 105, 415-426.

Qiu, Z., Zhao, X., Li, P., Zhang, X., Ali, S., Tan, J., 2015. Theoretical investigation of the energy performance of a novel MPCM (Microencapsulated Phase Change Material) slurry based PV/T module. *Energy* 87, 686-698.

R. Turns, S., 2006. *Thermodynamics. Concepts and applications*.

Stojanović, B., Akander, J., 2010. Build-up and long-term performance test of a full-scale solar-assisted heat pump system for residential heating in Nordic climatic conditions. *Applied Thermal Engineering* 30(2-3), 188-195.

Tsai, H.-L., 2015. Modeling and validation of refrigerant-based PVT-assisted heat pump water heating (PVTa-HPWH) system. *Solar Energy* 122, 36-47.

725 Wolf, M., 1976. Performance analyses of combined heating and photovoltaic power systems for
726 residences. *Energy Conversion* 16(1), 79-90.
727 Zhou, C., Liang, R., Zhang, J., Riaz, A., 2019. Experimental study on the cogeneration performance
728 of roll-bond-PVT heat pump system with single stage compression during summer. *Applied*
729 *Thermal Engineering* 149, 249-261.
730
731
732

Performance analysis of solar assisted heat pump coupled with build-in PCM heat storage based on PV/T panel

Jian YAO ^{a, b}, Hui XU ^{a, b}, Yanjun DAI ^{a, b, *}, Mingjun HUANG ^c

^a Institute of Refrigeration and Cryogenics, Shanghai Jiao Tong University, Shanghai 200240, China

^b Engineering Research Center of Solar Power and Refrigeration, MOE, China

^c Centre for Sustainable Technologies, School of the Built Environment, University of Ulster, Newtownabbey, Northern Ireland, BT37 0QB, UK

E-mail address: yjdai@sjtu.edu.cn (Yanjun DAI); Tel.: +86-21-34204358; fax: +86-21-34206814

Abstract

PV/T (photovoltaic/thermal) technology is a combination of PV module (photovoltaic utilization) and collector (photothermal utilization), which can improve the comprehensive utilization efficiency of solar energy and has a broad application prospect. In this paper, PV/T module is coupled with heat pump evaporator to form a direct-expansion solar PV/T heat pump which is suitable for heat application in high latitude area. To achieve stable residential heating, a solar PV/T heat pump system coupled with build-in PCM (phase change material) heat storage is therefore proposed and simulated. Meanwhile, the mathematical model of solar PV/T heat pump coupled with build-in PCM heat storage system is established and verified. The simulation results show that the temperature of underfloor heating which using build-in PCM heat storage can reach 22 °C to 31 °C after 39 hours when the circulating water is 40 °C. Moreover, the heating COP (Coefficient of Performance) increases with the increase of solar radiation, ambient temperature and area of PV/T collector, and decrease of wind speed, respectively. A 20 m² PV/T panel module can output 21.4% of the electricity to power grid when the solar radiation intensity is 600 W/m² and meet the heat demand of a 100 m² room while maintain the operation of the system. Meanwhile, the heating COP can reach 5.79 which is 70% higher than the conventional air conditioning system and the electrical, thermal, overall efficiencies are 17.77%, 55.76% and 75.49%, respectively.

1 Introduction

The total amount of energy consumption in the world is constantly climbing (2019; Caetano et al., 2017). The consumption of fossil energy has brought about energy crisis and environmental crisis (Pietrosemoli and Rodríguez-Monroy, 2019). Without action, CO₂ emissions from burning fossil fuels will be doubled by 2050 (Paolo Frankl, 2010). Therefore, the development and utilization of renewable energy has become one of the effective solutions (Keček et al., 2019). Solar energy has become the first choice due to its characteristics of ubiquity, abundance and sustainability (Kuik et al., 2019; Tsai, 2015), which is mainly used in two ways: photothermal and photovoltaic. 11% of global electricity will be provided by PV by 2050 (Paolo Frankl, 2010). However, the electrical efficiency of PV cells decreases with the increase of the temperature of PV cells (Huide et al., 2017). A cooling system can be added to reduce the temperature of PV cells while the remaining heat of PV panel are absorbed by working fluid which can be employed as a useful thermal energy for heat applications in buildings.

The PV/T technology coupled PV modules with thermal collectors was first proposed by Wolf et al (Wolf, 1976) to reduce PV cells temperature and improve electrical efficiency. The PV/T system can recover waste heat from the PV panel to improve comprehensive energy utilization efficiency. PV/T design optimizations are carried out to improve the system efficiency in recent years. Nahar et al. (Nahar et al., 2017) designed a novel pancake-shaped flow channel for PV/T system, and integrated the flow channel with the PV baseboard. They found that the temperature of the PV panel is reduced by 42 °C, and the electrical efficiency is increased by 2%. Othman et al. (Othman et al., 2016) proposed a parallel, double pass flat plate collector which was adopted in a two fluids PV/T system. Their results showed that the electrical efficiency and thermal efficiency are 17% and 76%, respectively.

The combination of PCM and PV/T panel is an effective way to stabilize the operating temperature of PV cells and improves the overall efficiency. Hosseinzadeh et al. (Hosseinzadeh et al., 2018) investigated the effect of simultaneous use of nanofluid as coolant as well as an organic paraffin as the phase change material on the electrical and thermal efficiencies. They demonstrated that the use of PCM in nanofluid based PVT/PCM system enhances the thermal output power of conventional PV/T system by 29.6%. Kazemian et al. (Kazemian et al., 2019) developed and simulated a comprehensive three-dimensional model of PV/T system integrated with PCM. Their simulation results presented that the PV/T-PCM system have lower surface temperature compared to PV/T system, and as the thermal conductivity of PCM enhances, both electrical and thermal efficiencies increase. Fayaz et al. (Fayaz et al., 2019) investigated the PCM based PV/T system, and the experimental validation was carried out to verify the numerical model. They found that the electrical efficiency is achieved as 13.98% and 13.87% numerically and experimentally respectively, and the electrical performance is improved as 6.2% and 4.8% for PV/T-PCM system based on the numerical and experimental results respectively.

Different working fluids like water, air, nanofluid and refrigerant are also used to cool the PV module. Huang and Lee (Huang and Lee, 2004) conducted long-term tests on the direct-expansion solar heat pump which adopted refrigerant as working fluid to verify the stability of the work. The total running time of their prototype is over 20000 hours, and the measured energy consumption is 0.019 kWh/l of hot water at 57 °C which is much less than traditional solar water heater. Stojanović and Akander (Stojanović and Akander, 2010) used direct-expansion heat pump for independent buildings heating and domestic hot water supply. In their system, the collector area is 42.5 m² and heat pump power is 8.4 kW, they measured that the actual indoor temperature is no less than 20 °C during the testing period. Alejandro Del Amo et al. (Del Amo et al., 2019) verified the feasibility of solar PV/T heat pump through experiments. They obtained that the highest COP of the system can reach 4.62. Meanwhile, the PV module provides 67.6% of the power demand, and the payback period is 6 years.

In addition to optimize the PV/T panel, the adoption of PCM as heat storage is also a good way to stabilize the system. Kuznik et al. (Kuznik et al., 2008) adopted PCM wallboard heat storage and conducted comparative experiments. In their study, the system can effectively reduce heat loss, keep the room warm and improve indoor thermal comfort. Fiorentini et al. (Fiorentini et al., 2015) combined PCM storage with PV/T system, and the roof was used as PV/T layout location. The PCM storage adopted in their system can keep indoor comfort within a certain and potentially variable thermal comfort range. Diallo et al. (Diallo et al., 2019) proposed the PVT-LHP (PVT Loop Heat Pipe) technology employing PCM triple heat exchanger, the total

energy efficiency of the presented system is improved by 28%, and the heating COP is 2.2 times than that of a traditional PV/T system.

Owing to the instability of solar energy, traditional solar PV/T system cannot continuously and stably supply heat or power generation when solar irradiation is weak such as rainy day or winter. Consequently, the market of PV/T technology compared with PV or PT system is still very low. PV/T can adapt to the characteristics of low intensity, instability and intermittency of solar energy better if it can be combined with accumulator and heat storage. However, additional space is required to install heat storage tank, which is not suitable for use in urban areas where land resources are scarce. Therefore, in this paper, a coupling design of solar PV/T heat pump and build-in PCM heat storage is proposed and the parallel air source heat exchanger is also adopted to enhance the stability of the system. The build-in PCM heat storage used for underfloor heating is a combination of PCM and building materials, which can save more space compared to conventional PCM storage tank system. Firstly, the composition and operation modes of the system are introduced. According to the system principle, the mathematical model is established and verified, and the build-in PCM heat storage sub-system which using for residential heating is also proposed and simulated. Then the influences of different parameters on system performance are analyzed. Finally, the feasibility analysis of the system is conducted. The objective of this paper is to provide a promising method to realize stable, high efficiency, environmental friendly residential heating in high latitude area with no energy consumption from power grid.

2 System description

Fig. 1 shows the schematic diagram of the system based on solar PV/T heat pump, which is consisted of four main parts: solar PV/T heat pump module, parallel air source heat pump module, heat storage module and electrical module. The blue lines represent low temperature working fluid, and in the opposite, red lines represent high temperature. The yellow lines represent the electricity flow direction. The arrows show the working fluid direction. The system can be divided into two operating modes, which are listed as follows.

(1) Sunny day operating mode: The electricity generated by PV panel is used to drive the pumps and compressor, and the excess electricity will be recovered to the power grid or drive the air conditioning. However, the PV panel heated by solar radiation will be resulted in an increase of the temperature of PV cells. Meanwhile, the heat transferred by the PV/T collector can be absorbed by the refrigerant. Then, the superheated refrigerant vapor with low pressure is compressed by the compressor to the high temperature and pressure refrigerant vapor. The condensation heat will be absorbed and stored in the build-in PCM heat storage. The heat transferred by condensation can also be used for producing domestic hot water. The liquid refrigerant will expand through the throttle valve after condensation process, and flow into the PV/T collector/evaporator. The heat released from the heat storage module will be used to keep the indoor temperature constant during the night.

(2) Rainy day operating mode: The system will switch to the air source heat pump mode when the solar radiation is insufficient to maintain system operation. The pumps and compressor driven by power grid are used to keep the system work. The air fan heat exchanger is adopted to absorb heat from the ambient air. The refrigerant will be heated by the air fan heat exchanger and compressed by compressor into high temperature and pressure vapor. The heat released by the refrigerant vapor will be transferred to the PCM or water. This mode can make full use of the

valley electricity to store heat at night, and maintain the indoor temperature through the heat storage module during the day.

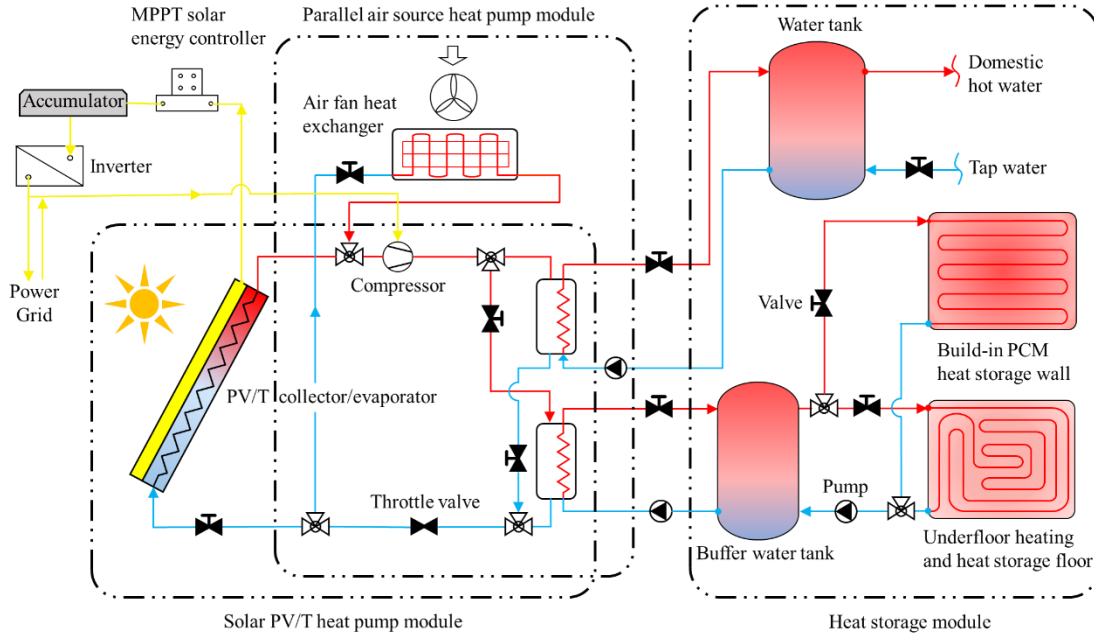


Fig. 1. Schematic of the system based on solar PV/T heat pump.

3 Mathematical model

The thermodynamic state points for each process are shown in Fig. 2. The solar PV/T heat pump cycle could be simplified to four components: PV/T collector/evaporator, compressor, PCM heat exchanger and throttle valve. Different temperature (T) and enthalpy (h) at each state point are shown in Fig. 2. Q_{th} (W) is the heat transfer rate between refrigerant and the PV/T panel, Q_e (W) is the electrical power provided by PV panel, and Q_{PCM} (W) is the heat transfer rate between refrigerant and phase change materials.

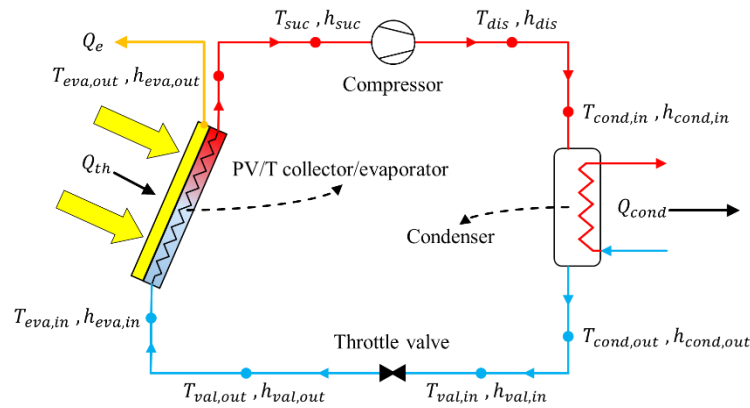


Fig. 2. The thermodynamic state points for each component.

The design parameters of the system and characteristics of different PV/T layers are listed in Table. 1.

Table. 1. Design parameters of the system and characteristics of different PV/T layers.

Parameters	Nomenclature	Value	Unit
------------	--------------	-------	------

Thickness of PV-glazing cover	$\delta_{g,pv}$	1	mm
Emissivity of PV-glazing cover	ε_c	0.84	[-]
Transmissivity of PV-glazing cover	$\tau_{g,pv}$	0.9	[-]
Thickness of PV cells	δ_{pv}	0.3	mm
Emissivity of PV cells	ε_p	0.96	[-]
Absorptance of PV cells	a_p	0.85	[-]
Thermal conductivity of PV cells	κ_p	203	W/m·K
Absorptance of PV baseboard	a_b	0.8	[-]
Thickness of EVA grease	δ_{EVA}	0.5	mm
Thermal conductivity of EVA grease	κ_{EVA}	0.311	W/m·K
Thickness of electrical insulation	δ_{ei}	0.5	mm
Thermal conductivity of electrical insulation	κ_{ei}	0.15	W/m·K
Electrical insulation material	[-]	Tedlar	[-]
Packing factor	β_p	1	[-]
Length of PV/T collector/evaporator	L	2.0	m
Width of PV/T collector/evaporator	W	1.0	m
Area of the PV/T collector/evaporator	A	2.0	m ²
Thermal conductivity of roll-bond panel	κ_{rb}	151	W/m·K
Thickness of roll-bond panel pipe	δ_{rb}	1	mm
Refrigerant type	ref	R134A	[-]

3.1. Model of PV/T collector/evaporator

The heat absorbed by the PV/T panel is expressed as follows:

$$Q_{abs} = (1 - \eta_e) \cdot A \cdot I \cdot \tau_{g,pv} \cdot [\alpha_p \cdot \beta_p + \alpha_b \cdot (1 - \beta_p)] \quad (1)$$

where A is the collector area of the PV/T panel (m²); I is the solar radiation intensity (W/m²); $\tau_{g,pv}$ is the transmittances of the PV-glazing cover; α_p and α_b are the absorption ratios of the PV cells and its baseboard, respectively; β_p is the packing factor of PV cells; η_e is the PV cells' efficiency, calculated by (Huide et al., 2017):

$$\eta_e = \eta_{rc} \cdot [1 - \beta_{pv} \cdot (T_p - T_{rc})] \quad (2)$$

η_{rc} is the reference photovoltaic efficiency value of PV cells at $T_{rc}=298$ K, $\eta_{rc}=0.18$; β_{pv} is the temperature coefficient (1/K) of PV cell efficiency, $\beta_{pv}=0.0045$ (Huide et al., 2017).

Fig. 3 shows the heat loss and physical model of PV/T panel which has a multi-layer structure, the heat loss of PV/T panel consists of two parts: (1) heat transfer from PV cells to PV-glazing cover; (2) heat transfer from PV-glazing cover to ambient air.

The total heat loss rate of PV/T module is given as:

$$Q_L = U_L \cdot A \cdot (T_p - T_a) \quad (3)$$

where T_p and T_a are the temperature of PV cells and ambient air, respectively. U_L is the overall heat loss coefficient which can be written as:

$$U_L = \left[1 / (h_{cv,p-c} + h_{rd,p-c}) + 1 / (h_{cv,c-a} + h_{rd,c-a}) \right]^{-1} \quad (4)$$

$h_{cv,p-c}$ and $h_{rd,p-c}$ are the convective and radiative heat-transfer coefficients between PV cells and glass cover; $h_{cv,c-a}$ and $h_{rd,c-a}$ are the convective and radiative heat-transfer coefficients between glass cover and ambient.

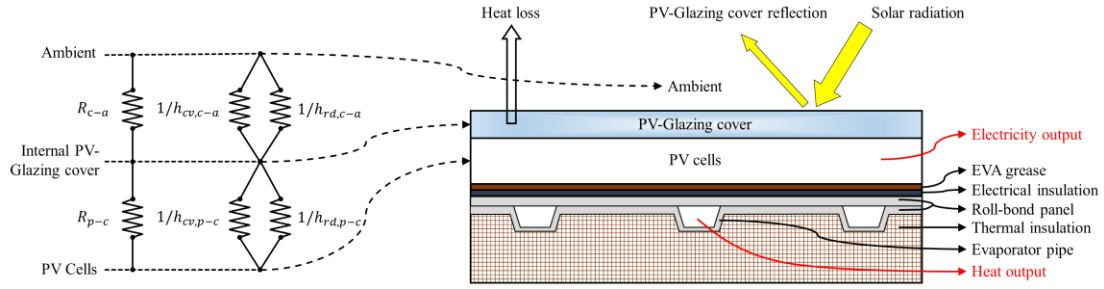


Fig. 3. Heat loss and physical model of PV/T collector/evaporator.

The overall electricity output power of PV cells is given as:

$$Q_e = A \cdot I \cdot \tau_{g,pv} \cdot \alpha_p \cdot \beta_p \cdot \eta_e \quad (5)$$

Under the steady-state condition, the heat transfer rate delivered by the module equals the rate of the absorbed heat minus the overall heat loss, expressed as:

$$Q_{th} = Q_{abs} - Q_L \quad (6)$$

The total useful solar heat received by the PV/T collector/evaporator is expressed as:

$$Q_u = F_R \cdot A \cdot I \cdot \tau_{g,pv} \cdot [\alpha_p \cdot \beta_p + \alpha_b \cdot (1 - \beta_p)] \quad (7)$$

where F_R is the PV/T collector thermal efficiency factor, can be defined as (Diallo et al., 2019):

$$F_R = (1 - \eta_e) \cdot \frac{1/U_L}{L \cdot W / N_{rb} \cdot \left\{ 1 / \left(L \cdot U_L - \left[(W / N_{rb} - L_{rb}) F_{rb} + L_{rb} / (1 + R_{pv} \cdot U_L) \right] \right) + \sum_1^5 R_i \right\}} \quad (8)$$

N_{rb} is the equivalent number of roll-bond panel pipe; L_{rb} is the equivalent length of roll-bond panel pipe; $\sum R_i$ is the overall thermal resistance from the PV cells to the PCM; F_{rb} is the efficiency of the roll-bond panel which encapsulated in the backside of the PV/T panel which can be defined as (Diallo et al., 2019):

$$F_{rb} = \tanh \left[\frac{\sqrt{\frac{U_L}{(k_{rb} \delta_{rb} (1 + R_{pv} U_L))}} (W / N_{rb} - L_{rb}) / 2}{\sqrt{\frac{U_L}{(k_{rb} \delta_{rb} (1 + R_{pv} U_L))}} (W / N_{rb} - L_{rb}) / 2} \right] \quad (9)$$

κ_{rb} is the thermal conductivity of roll-bond panel; δ_{rb} is the thickness of the roll-bond panel pipe; R_{pv} is the thermal resistance of PV cells.

The thermal resistances of the PV/T system and heat transfer along the system are shown in Fig. 4.

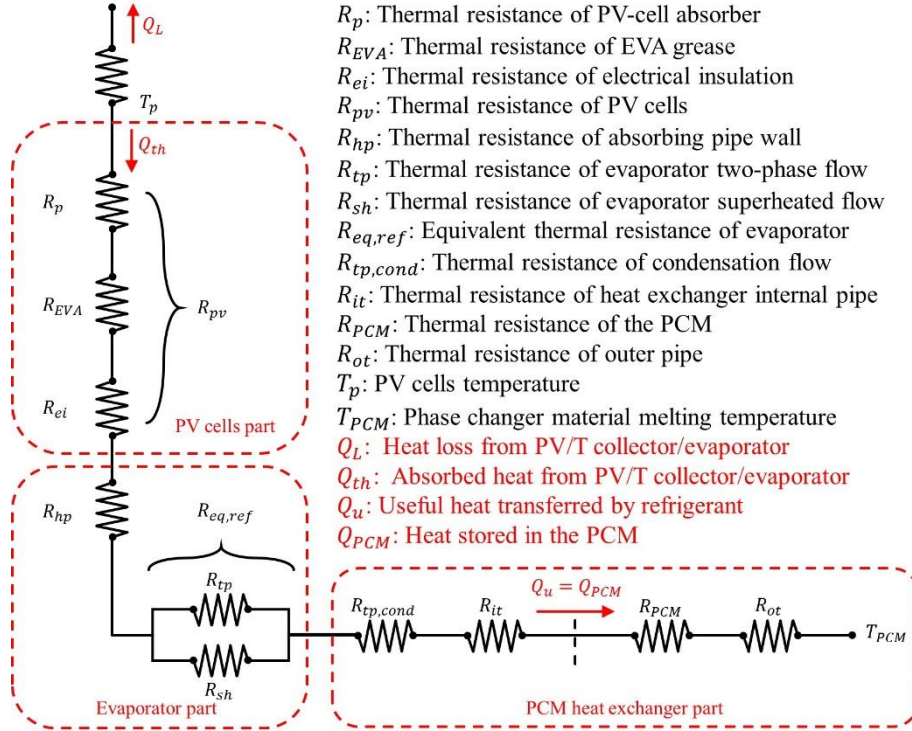


Fig. 4. Thermal resistances of the PV/T system and heat transfer along the system.

Heat transfer between PV module and heat pipe is a conventional one dimensional heat conduction process and its associated thermal resistance is:

$$R_{pv} = \delta_p / k_p + \delta_{EVA} / k_{EVA} + \delta_{ei} / k_{ei} \quad (10)$$

Superheated region and two-phase region existed in the refrigerant side of the PV/T collector/evaporator. The equivalent thermal resistance of the two different regions can be calculated as (P. Hartnett and M. Rohsenow, 1973):

$$R_{eq,ref} = \left(1/R_{tp} + 1/R_{sh} \right)^{-1} \quad (11)$$

3.2. Model of build-in PCM heat storage

All the heat gained by the build-in PCM heat storage is transferred by the PCM heat exchanger. The heat store rate in the PCM and concrete is expressed as follows:

$$Q_{PCM} + Q_{conc} = \dot{m}_{ref} \cdot (h_{dis} - h_{in}) \quad (12)$$

The PCM melting rate is calculated by:

$$\dot{m} = Q_{PCM} / \Delta H_{PCM} \quad (13)$$

where ΔH_{PCM} is the latent heat of the PCM (kJ/kg).

Fig. 5 shows the phase change temperature of 15 kinds of phase change materials including organic/inorganic/eutectic compounds materials. According to L.F. Cabeza et al. (Cabeza et al., 2011), the recommendation phase change temperature range for underfloor heating is between 30 °C to 40 °C. There are five kinds of PCM that have phase change temperature in this range:

Paraffin wax, $\text{CaCl}_2 \cdot (\text{H}_2\text{O})_6$ - $\text{MgCl}_2 \cdot (\text{H}_2\text{O})_6$, Calcium chloride hexahydrate, Sodium sulphate decahydrate, Sodium phosphate dibasic dodecahydrate.

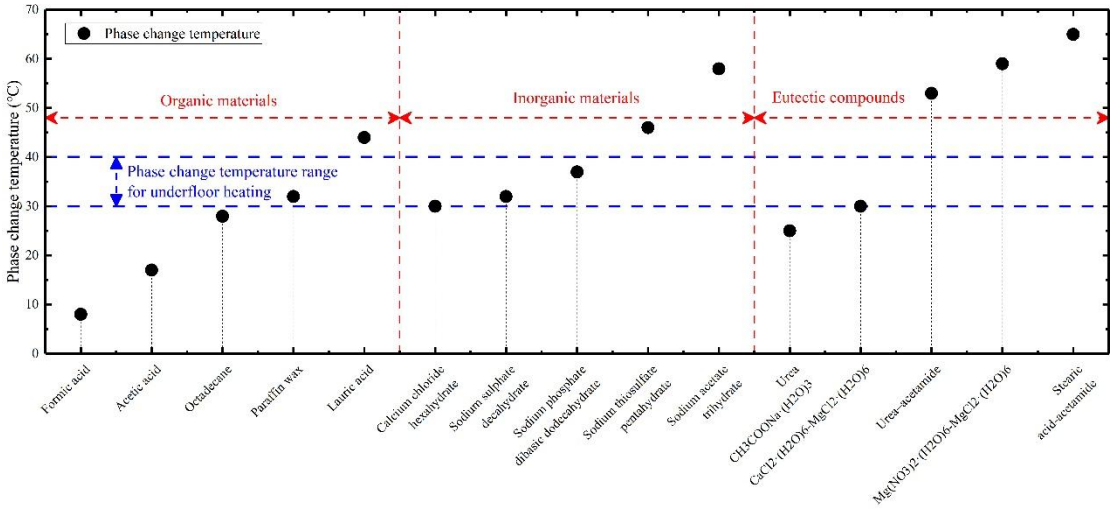
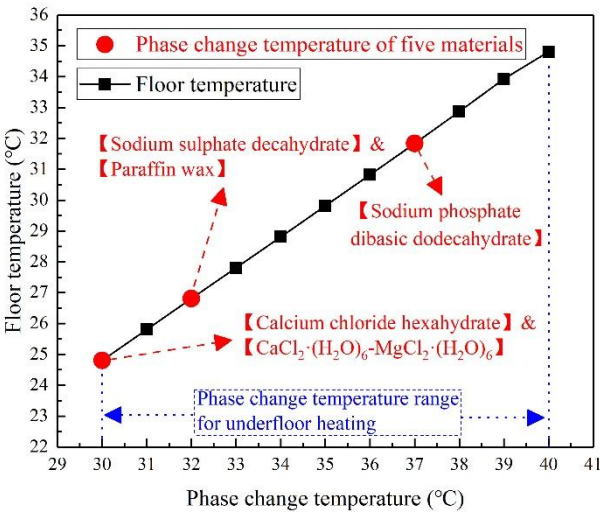


Fig. 5. Phase change temperature of 15 kinds of PCM including Organic/Inorganic/Eutectic compounds materials.

The variation curve of floor temperature with phase change temperature and the comparison of three indices including thermal conductivity, latent heat and price (Pereira da Cunha and Eames, 2016) of above five kinds of PCM are shown in Fig. 6. These five materials have different phase change temperature which all in the recommendation temperature range for underfloor heating. The ideal material should have a higher thermal conductivity and latent heat while the price is low. In order to evaluate these five materials, the graph of ideal material is also plotted in Fig. 6. The organic and eutectic compounds phase change materials have a higher price than inorganic materials while the thermal conductivity and latent heat are lower. Moreover, the larger of the overlap area in Fig. 6 between each material and ideal material, the better of the material performance. As shown in Fig. 6, Sodium phosphate dibasic dodecahydrate has the largest overlap area, thus, it is used in the simulation of build-in PCM heat storage unit.



(a)

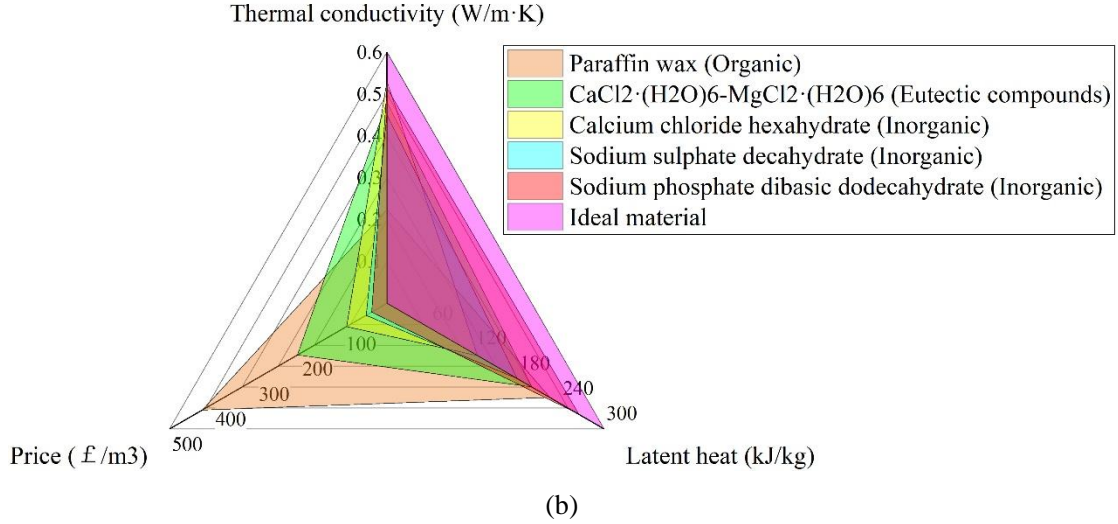


Fig. 6. (a) Variation curve of floor temperature with phase change temperature. **(b)** Thermal conductivity/Latent heat/Price comparison of six kinds of materials including ideal material.

Fig. 7 illustrates the structure and cross-section view of a build-in PCM heat storage unit which is the component of underfloor heating module. The phase change materials (Sodium phosphate dibasic dodecahydrate) are placed in the outer tube of a double-wall tube which can store heat during the day and release latent heat at night. Polystyrene board and foam concrete are used as thermal insulation and building materials, respectively. The hot water which produced by solar PV/T heat pump module is pumped into the pipe of underfloor heating to keep the indoor temperature steady. The properties of PCM (Jankowski and McCluskey, 2014) and concrete as well as underfloor heating working conditions are listed in Table. 2.

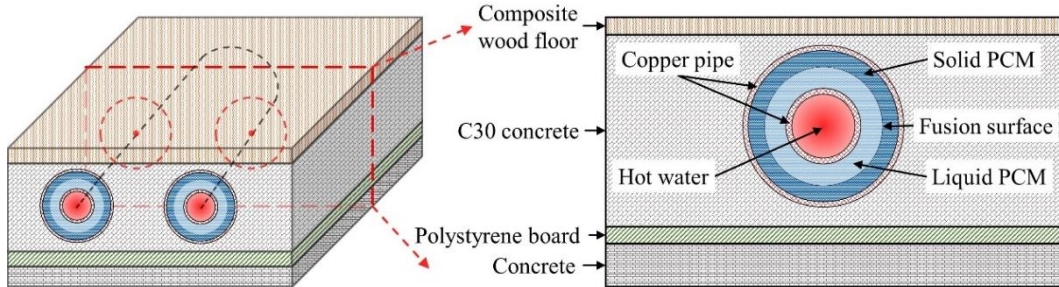


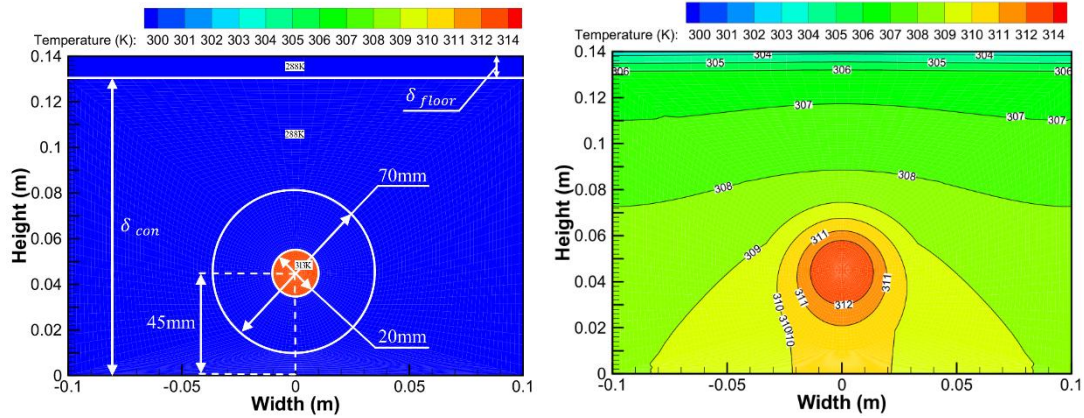
Fig. 7. Structure and cross-section view of the build-in PCM heat storage unit.

Table. 2. Properties of PCM and concrete as well as underfloor heating working conditions.

Parameters	Nomenclature	Value	Unit
Type of PCM	$[-]$	$\text{Na}_2\text{HPO}_4 \cdot 12\text{H}_2\text{O}$	$[-]$
Latent heat of PCM	ΔH_{PCM}	265	kJ/kg
Density of PCM	ρ_{PCM}	1507	kg/m ³
Temperature of transition of PCM	T_{mel}	37	°C
Specific heat at constant pressure of PCM	C_{p-PCM}	1.69	kJ/kg·K
Thermal conductivity of PCM	κ_{PCM}	0.514	W/m·K
Thermal conductivity of copper coil	κ_C	397	W/m·K

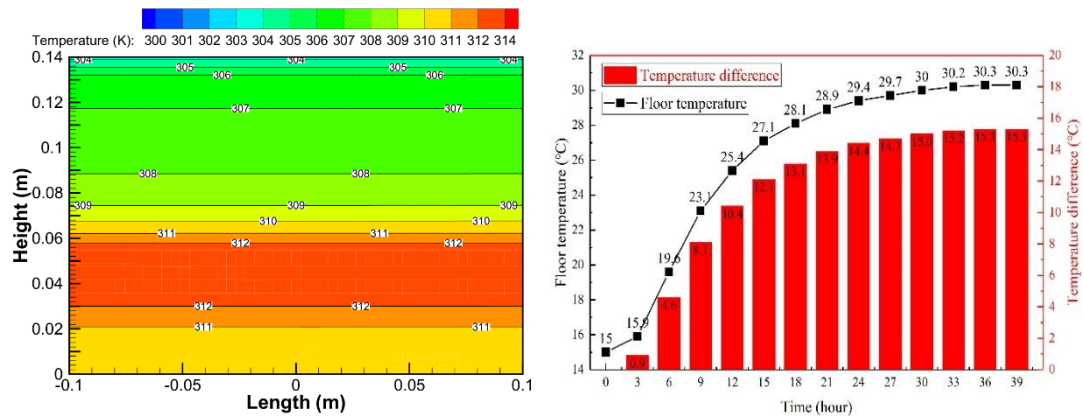
Type of concrete	$[-]$	C30	$[-]$
Specific heat at constant pressure of concrete	C_{p-conc}	0.97	$\text{kJ/kg}\cdot\text{K}$
Thermal conductivity of concrete	κ_{con}	1.6	$\text{W/m}\cdot\text{K}$
Density of concrete	ρ_{conc}	2300	kg/m^3
Thickness of the concrete	δ_{con}	0.13	m
Thickness of the wood floor	δ_{floor}	0.01	m
Volume flow rate of circulating water	V_{cw}	2.5	m^3/h

Fig. 8 (a~c) presents the simulation results of heat transfer in build-in PCM heat storage unit at different time which carried out by software of Ansys Fluent 17.0. The thermal conductivity of the heat transfer between the coil and PCM has been considered in the setup of the boundary conditions. Thus, the boundary conditions of inner and outer tube have been set as “coupled” in Ansys Fluent 17.0 which means the solution of heat transfer process would be carried out through the coupled method in the program. The initial temperature of the heat storage unit is 15 °C, and the underfloor heating can reach above 30 °C after 39 hours when the circulating water is 40 °C. As shown in Fig. 8(d), the floor temperature increases with time and reaches 25 °C in the first 12 hours which has 10 °C difference with the ambient. The changing curve mountains rapidly in the initial stage and becomes steady after 39 hours, the build-in PCM heat storage would supply heat to indoor area and maintain the room temperature.



(a) Initial stage

(b) Steady stage



(c) Cross-section view at the width of 0 (steady stage)

(d)

Fig. 8. (a~c) Cross-section temperature contour of the build-in PCM heat storage unit at initial and steady stage. **(d)** Variation curve of floor temperature and temperature difference between floor and ambient.

Fig. 9 shows the variation curves of circulating water temperature and floor temperature with the length of circulating water tube. The temperature of circulating water would decrease from 40 °C (inlet) to 32.5 °C (outlet) while the floor temperature varies from 30.4 °C to 22.9 °C. This figure also presents the three temperature range of underfloor heating which can divided into three categories: Temperature range of no person staying area (29 °C-35 °C), Temperature range of short-time staying area (25 °C-29 °C) and Temperature range of long-time staying area (20 °C-25 °C). Therefore, when using build-in PCM heat storage as underfloor heating, the system could meet the heat demand of users and keep indoor temperature steady.

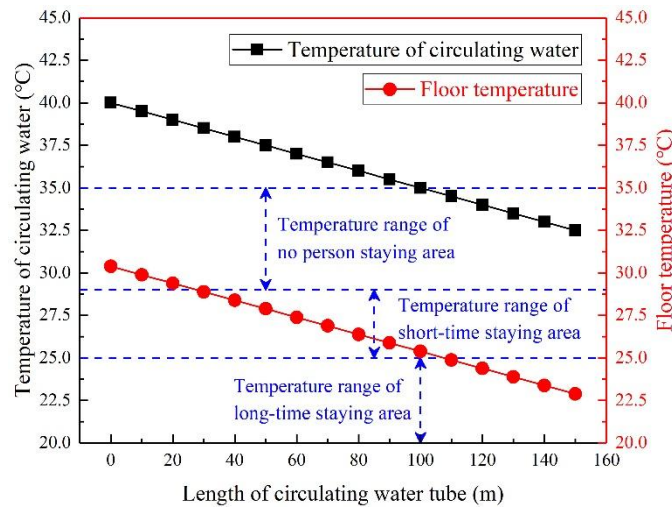


Fig. 9. Variation curves of circulating water temperature and floor temperature with the length of circulating water tube.

3.3. Model of compressor

The refrigerant mass flow rate \dot{m}_{ref} could be calculated by (Ma, 2013)

$$\dot{m}_{ref} = \lambda \cdot V_{th} / v_{suc} \quad (14)$$

where the λ is the compressor volumetric efficiency, V_{th} is the theoretical displacement volume of compressor (m^3), v_{suc} is the specific volume of the refrigerant in the suction period (m^3/kg).

The power consumption of compressor is written as:

$$P_{com} = \dot{m}_{ref} \cdot (h_{dis} - h_{suc}) / \eta_{ele} \quad (15)$$

where η_{ele} is the efficiency of the compressor which can be expressed by (Ma, 2013):

$$\eta_{ele} = -0.17938 + 0.87501 \frac{p_{dis}}{p_{suc}} - 0.30014 \left(\frac{p_{dis}}{p_{suc}} \right)^2 + 0.04135 \left(\frac{p_{dis}}{p_{suc}} \right)^3 - 0.00206 \left(\frac{p_{dis}}{p_{suc}} \right)^4 \quad (16)$$

The refrigerant vapor through compressor is isentropic, thus the equation can be expressed by:

$$T_{dis} / T_{suc} = (p_{dis} / p_{suc})^{(\chi-1)/\chi} \quad (17)$$

where the χ is the polytropic index of refrigerant. h_{dis} is the enthalpy of the vapor after compressed (kJ/kg), h_{suc} is the enthalpy of the vapor before compressed (kJ/kg).

The heat of refrigerant absorbed from the PV/T collector/evaporator equal to Q_u :

$$\dot{m}_{ref} \cdot (h_{eva,out} - h_{eva,in}) = Q_u = Q_{th} \quad (18)$$

3.4 Definition of the system performance

The COP (Coefficient of Performance) of the system can be defined as the ratio of overall heat output of system and power consumption of the compressor as following (R. Turns, 2006)

$$COP = \dot{m}_{ref} \cdot (h_{cond,in} - h_{cond,out}) / P_{com} \quad (19)$$

The η_{th} is the PV/T collector/evaporator's thermal efficiency, which can be defined as:

$$\eta_{th} = Q_{th} / (A \cdot I) \quad (20)$$

The η_e is the PV cells electrical efficiency which can be defined as:

$$\eta_e = Q_e / (A \cdot I) \quad (21)$$

The η_{ove} is the overall efficiency which can be defined as:

$$\eta_{ove} = (Q_{cond} + Q_e) / (A \cdot I) \quad (22)$$

3.5 Presentation of the algorithm by flow chart

The numerical simulation procedure of the system is shown in Fig. 10 to predict the system performance using the software of MATLAB. The solution steps are as flows:

- (1) Input all the environmental parameters, such as solar radiation intensity, wind speed, ambient temperature, etc.
- (2) Input the system design parameters and operation parameters, such as collector area, packing factor, collector slop, transmissivity of external glass cover, PV-glazing cover, thickness of each layer, etc.
- (3) Assume the temperature of PV cells T_p .
- (4) Calculate the overall heat loss rate Q_L , and the PV electrical output power Q_e .
- (5) Calculate the thermal energy gain rate through PV/T collector/evaporator Q_{th} , and the useful heat transfer rate by refrigerant Q_u .
- (6) Calculate $(Q_{th} - Q_u)/Q_{th}$. If $|(Q_{th} - Q_u)/Q_{th}| < 0.1\%$, the system achieves the heat balance and move to next step.
- (7) Input the superheat degree T_{sh} .
- (8) Assume the compressor discharge pressure P_{dis} .
- (9) Calculate the PV/T collector/evaporator inlet enthalpy $h_{eva,in}$ and the PCM heat exchanger outlet enthalpy $h_{cond,out}$. If $|(h_{eva,in} - h_{cond,out})/h_{cond,out}| < 0.1\%$, the system achieves the

pressure balance and move to next step.

(10) Calculate the COP, PCM melting rate \dot{m} , thermal efficiency η_{th} , electrical efficiency η_e , and overall efficiency η_{ove} .

(11) Results output, and stop the program.

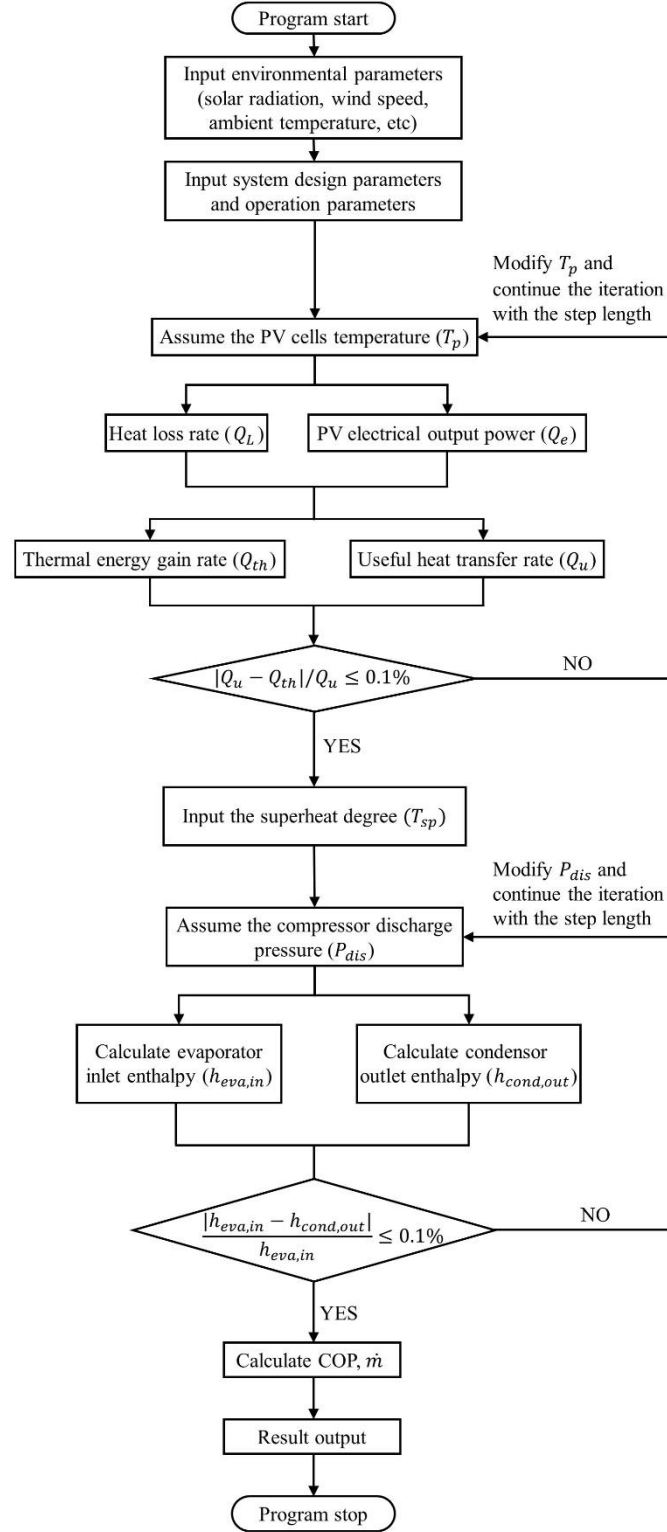


Fig. 10. Numerical solution procedure of the system.

4 Validation of the model

To ensure the reliability of the mathematic model, the simulation results should be compared with the experimental results. The experimental parameters used in the simulation are listed in Table. 3.

Table. 3. Experimental parameters (Zhou et al., 2019).

Parameters	Nomenclature	Value	Unit
Thickness of glass cover	δ_g	3.2	mm
Thickness of air gap	δ_{air}	35	mm
Thickness of PV-glazing cover	$\delta_{g,pv}$	1	mm
Thickness of PV cells	δ_{pv}	0.2	mm
Thickness of EVA adhesive film	δ_{EVA}	0.4	mm
Thickness of electrical insulation	δ_{ei}	0.5	mm
Length of PV/T	L	3.0	m
Width of PV/T	W	1.6	m
Wind speed	v_{wind}	1.5	m/s
Ambient temperature	T_a	298.5	K
Refrigerant type	ref	R22	[-]
Packing factor	β_p	0.64	[-]

The comparison results of heating COP are presented in Fig. 11(a), the operating conditions are refer from Zhou et al.(Zhou et al., 2019). Under the same system components (PV/T collector/evaporator, compressor, condenser, expansion valve, water tank), the simulation results are in good agreement with the experimental results. Heating COP of the PV/T system increases in the first 15 minutes because the water in the tank still in the low temperature range. Thus, the temperature differences between the refrigerant fluid and water remains large in the condenser leading to a high heat transfer efficiency. However, the heat transfer efficiency of the condenser would be decreased when the temperature of the inlet water rises up during the operation of the whole system. That is the reason of the reduction of heating COP after 15 minutes. The average error of heating COP is 2.84% while the maximum error is 5.12%. Fig. 11(b) presents the experimental and simulation results of the photovoltaic efficiency. The maximum photovoltaic efficiency is 10.11% while the minimum is 8.09%, but all the experimental photovoltaic efficiencies fluctuate around 9.24%. The simulation photovoltaic efficiencies remain around 9.25% but fluctuate from 9.01% to 9.7% due to the influence of solar radiation intensity. The average error of photovoltaic efficiency is 4.48% while the maximum error is 9.30%.

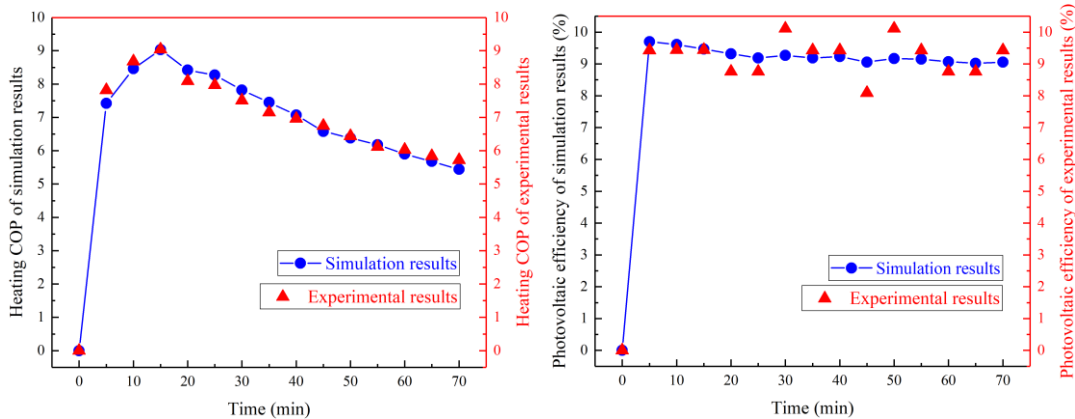


Fig. 11. (a) Comparison results of experimental and simulated heating COP. **(b)** Comparison results of experimental and simulated photovoltaic efficiency.

5 Parameter analysis

In this section, the influences of different parameters (solar radiation intensity, ambient temperature, wind speed, area of PV/T collector) on this system are investigated, and the performance indices of the system under typical working conditions are also given. It should be noted that when one parameter is varied, others keep constant. Pressure ratio of the compressor refers the ratio of pressure of discharged refrigerant vapor and charged refrigerant vapor.

5.1 Solar radiation intensity

The influences of solar radiation intensity which varying from 200 W/m² to 1000 W/m² are shown as follows at the working conditions are: ambient temperature is 25 °C, wind speed is 1.5 m/s and area of PV/T collector is 2 m².

Fig. 12 presents the rising curve of the heating COP and declining curves of thermal, electrical and overall efficiencies. The heating COP is 3.0 for a solar radiation of 200 W/m², and it can reach up to 10.8 when the solar radiation is 1000 W/m². The refrigerant evaporation temperature and pressure will be increased due to a higher temperature of PV cells. Thus, the compressor consumes less electricity to compress the refrigerant vapor leading to this upward trend. Meanwhile, the heat loss will mount due to a higher temperature difference between PV cells and ambient. Thereby, the thermal and electrical efficiencies of the PV/T panel reduce resulting in a reduction of the overall efficiency.

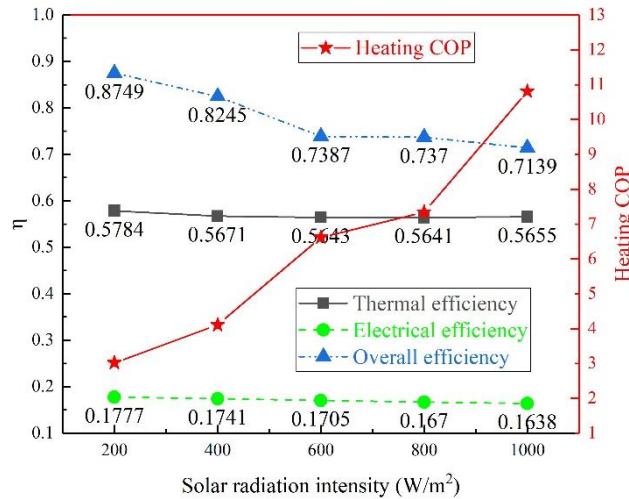


Fig. 12. Influence of solar radiation intensity on heating COP and thermal, electrical, overall efficiencies.

Fig. 13 shows the effect of solar radiation intensity on thermal and electrical output power, pressure ratio and mass flow rate of refrigerant. The thermal and electrical power keep mounting with the increase of the solar radiation intensity. Meanwhile, the pressure ratio of the compressor decreases and the mass flow rate of the refrigerant increases. That is because the increase of the

evaporation temperature causes a higher evaporation pressure which equals to the suction pressure of compressor leading to a lower pressure ratio. Furthermore, a larger amount of refrigerant will be needed to transfer extra heat from PV/T collector/evaporator to PCM heat exchanger (condenser) when the PV/T panel absorbs more heat from solar radiation.

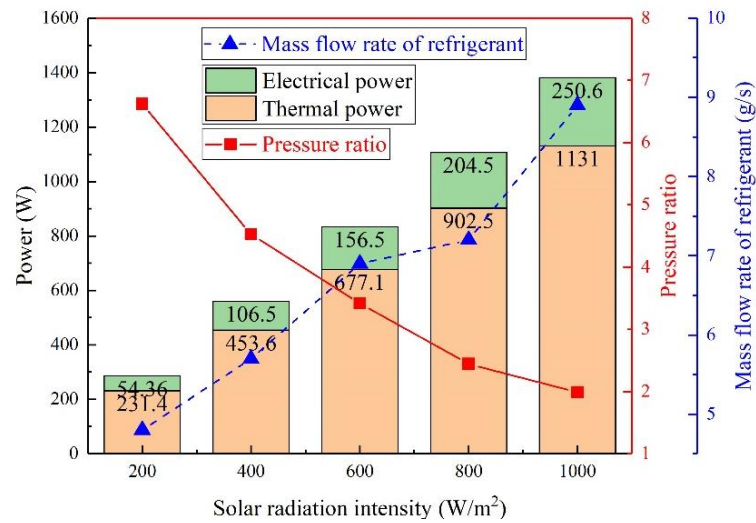


Fig. 13. Influence of solar radiation intensity on electrical and thermal power, pressure ratio and mass flow rate of refrigerant.

As shown in Fig. 14, there is a positive linear correlation between PV cells' electrical power generation and solar radiation intensity while the consumption power of compressor fluctuates around 120 W. When the output power to grid is less than zero, it means the system consumes electricity from the power grid. The electrical power generated by PV panels could meet the demand of the compressor and the system could output electricity to power grid when the solar radiation intensity exceeds 500 W/m².

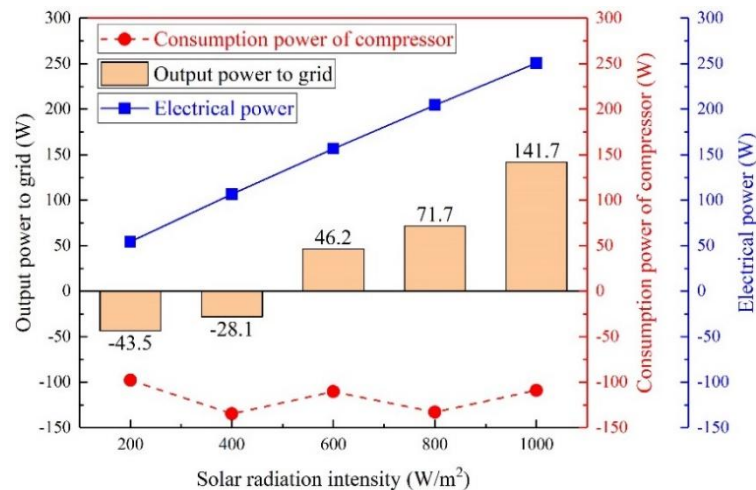


Fig. 14. Influence of solar radiation intensity on electrical power, consumption power of compressor and output power to grid.

5.2 Ambient temperature

The influences of ambient temperature which varying from 15 °C to 35 °C are shown as follows at the working conditions are: solar radiation intensity is 600 W/m², wind speed is 1.5 m/s

and area of PV/T collector is 2 m².

Fig. 15 shows that increasing the ambient temperature will increase the heating COP and thermal efficiency but decrease the electrical and overall efficiencies. The temperature difference between PV cells and ambient will reduce when the ambient temperature rises leading to a less heat loss from PV/T panel to the surrounding. Thus, the heating COP increases and the electrical efficiency decreases due to a higher temperature of the PV cells while the thermal efficiency increases. However, the electrical efficiency outweighs the thermal efficiency resulting in a reduction of the overall efficiency when the ambient temperature is below 25°C. The heating COP (9.25) at 35 °C is higher than COP (5.79) at 15 °C by 59.8%, thus a higher ambient temperature is better for the system performance.

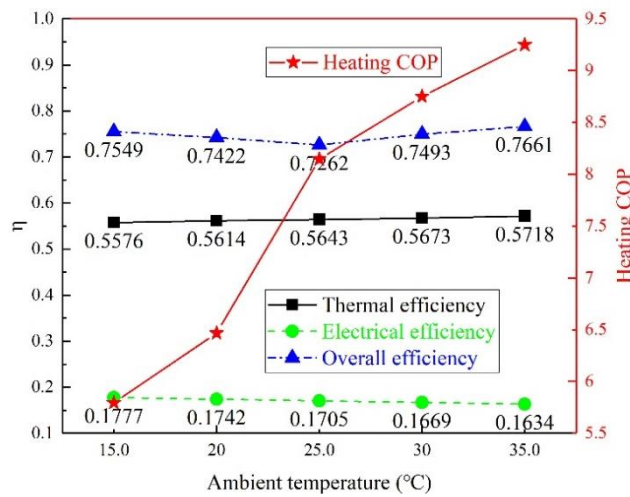


Fig. 15. Influence of ambient temperature on heating COP and thermal, electrical, overall efficiencies.

The variation curves of thermal and electrical power, pressure ratio and mass flow rate of refrigerant with the increase of ambient temperature are shown in Fig. 16. The changing curves of the electrical and thermal output power are the same as the electrical and thermal efficiencies. The pressure ratio of the compressor will increase when the ambient temperature is below 25 °C and decrease when the ambient temperature is over 25 °C. That is because a lower ambient temperature leads to a lower superheat degree of refrigerant which cause a lower pressure ratio, and in the opposite, a higher ambient temperature leads to a higher superheat degree. Moreover, when the ambient temperature exceeds 25 °C, it will influence the thermal efficiency of PV/T collector causing the reduction of pressure ratio. The mass flow rate of the refrigerant will keep climbing when the ambient temperature rises because less heat will lose in the ambient while more heat will be absorbed by refrigerant.

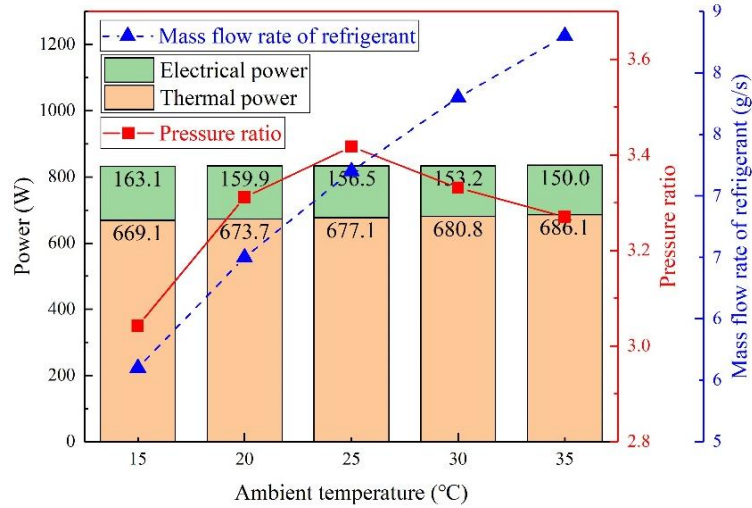


Fig. 16. Influence of ambient temperature on electrical and thermal power, pressure ratio and mass flow rate of refrigerant.

As shown in Fig. 17, the electrical power of PV decreases linearly with the ambient temperature while the consumption power of compressor decreases when the ambient temperature is below 25 °C and increases when the ambient temperature exceeds 25 °C. The output power to grid reaches its maximum at 25 °C. Because when the ambient temperature is below 25 °C, the effect of environmental heat loss is greater than that of heat-collecting efficiency due to a large temperature difference. However, the effect of a higher ambient temperature on heat-collecting efficiency is greater than that of environmental heat loss when the ambient temperature exceeds 25 °C.

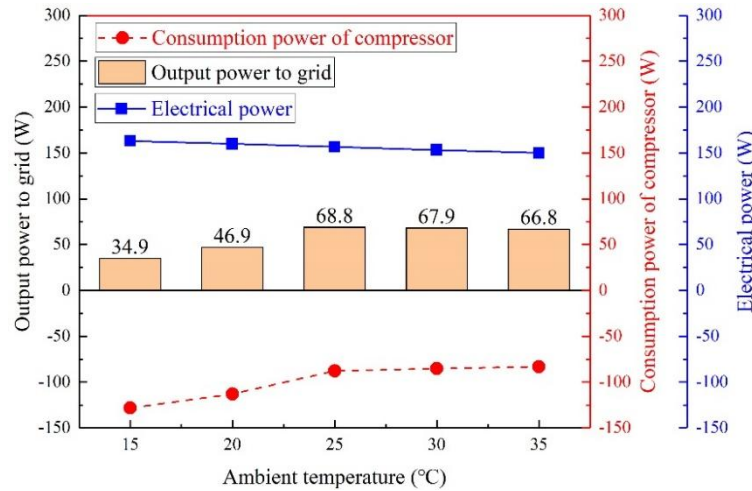


Fig. 17. Influence of ambient temperature on electrical power, consumption power of compressor and output power to grid.

5.3 Wind speed

The influences of wind speed which varying from 0.5 m/s to 2.5 m/s are shown as follows at the working conditions are: solar radiation intensity is 600 W/m², ambient temperature is 25 °C and area of PV/T collector is 2 m².

Fig. 18 shows the variation curve of heating COP, thermal, electrical and overall efficiencies

with wind speed varying from 0.5 m/s to 2.5 m/s. The heating COP will decrease rapidly when the wind speed is low and steadily when the wind speed increases. More heat will be transferred to the environment and less heat is absorbed by the PV/T panel under a higher wind speed. Meanwhile, evaporation temperature of refrigerant will be decreased and the consumption power of compressor will be increased when the temperature of PV cells rises. Thus, the heating COP drops from 9.4 to 6.8, which means better wind protection measures should be taken to improve the system performance.

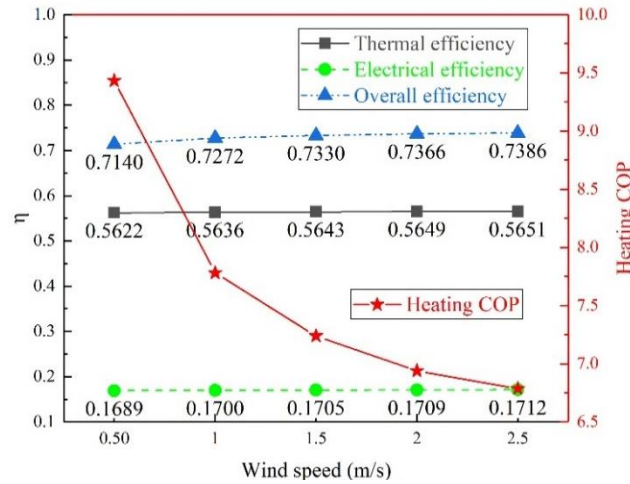


Fig. 18. Influence of wind speed on heating COP and thermal, electrical, overall efficiencies.

The variation curves of thermal and electrical power, pressure ratio and mass flow rate of the refrigerant with the increase of wind speed are shown in Fig. 19. The changing curves of the thermal and electrical power have the same trend as the thermal and electrical efficiencies. Both the pressure ratio and mass flow rate of refrigerant reduce with the increase of the wind speed. That is because more heat will be absorbed by the ambient air while less heat will be transferred by the refrigerant.

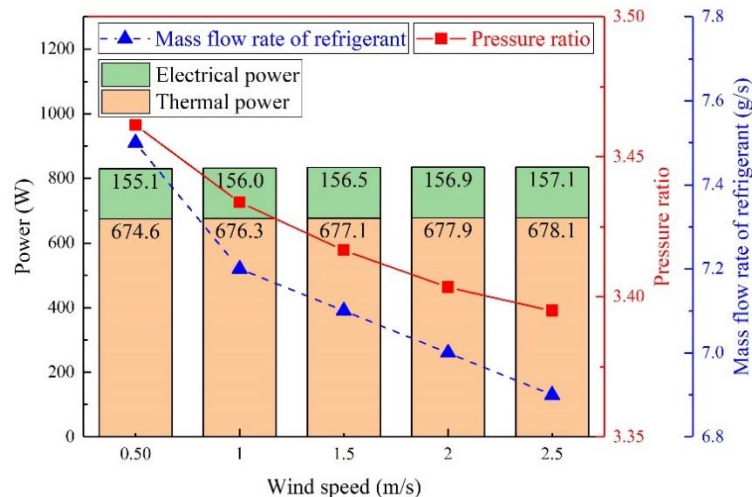


Fig. 19. Influence of wind speed on electrical and thermal power, pressure ratio and mass flow rate of refrigerant.

Fig. 20 presents the influence of wind speed on electrical power, consumption power of compressor and output power to grid. The output power to grid decreases rapidly when the wind

speed increases from 0.5 m/s to 1.5 m/s and steadily when the wind speed exceeds 1.5 m/s. More heat will loss in the environment due to a higher wind speed, and the thermal efficiency will decrease causing a higher consumption power of compressor.

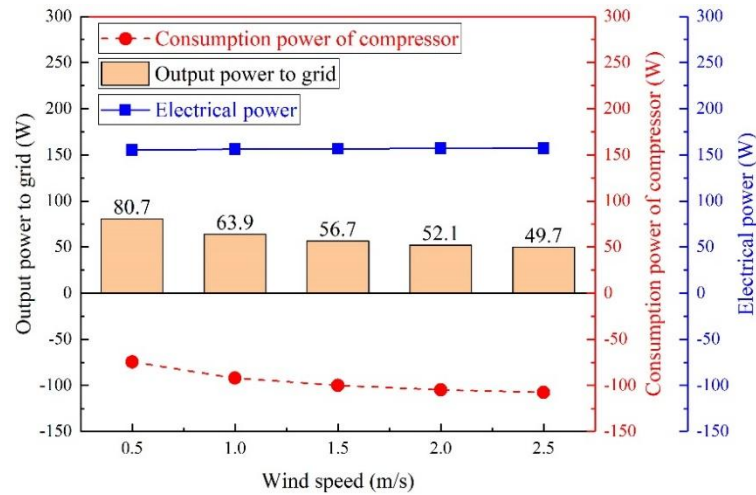


Fig. 20. Influence of wind speed on electrical power, consumption power of compressor and output power to grid.

5.4 Area of PV/T collector

The influences of the area of PV/T collector which varying from 1 m² to 3 m² are shown as follows at the working conditions are: solar radiation intensity is 600 W/m², ambient temperature is 25 °C and wind speed is 1.5 m/s.

Fig. 21 presents the influence of the area of PV/T collector on pressure ratio, heating COP and overall efficiency. Pressure ratio and overall efficiency reduce with the increase of the area, while the heating COP mounts. That is because a larger area can absorb more heat from the solar radiation, and the extra heat will be transferred by PV/T panel to refrigerant. Meanwhile, the evaporation temperature and pressure will increase leading to a lower pressure ratio and a higher heating COP. The consumption power of the compressor will decrease when the pressure ratio reduces, thus the heating COP increases more rapidly under large area conditions. A higher temperature of the PV cells causes more heat dissipates in the ambient resulting a decrease of the overall efficiency.

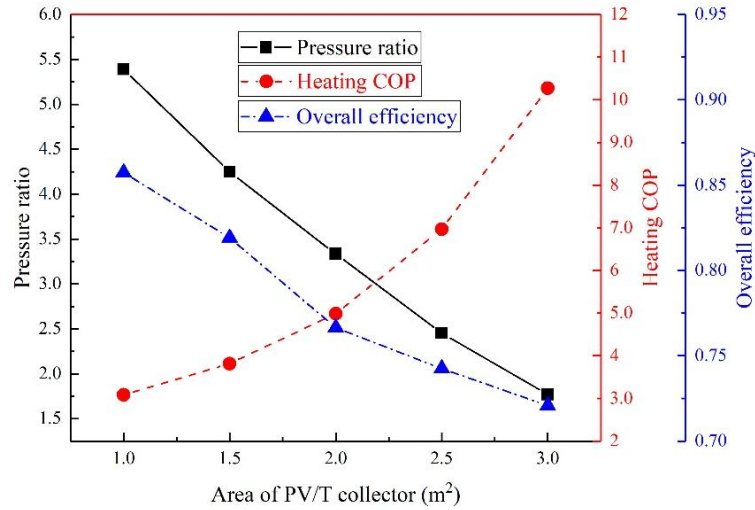


Fig. 21. Influence of the area of PV/T collector on pressure ratio, heating COP and overall efficiency.

Fig. 22 shows the declining trends of the pressure ratio and increasing trends of the thermal and electrical power influenced by the area of PV/T collector. The thermal and electrical output power are almost linearly and positively correlated with the area of PV/T collector. That is because more heat will gain from the solar radiation and be transferred to the refrigerant when the area increases.

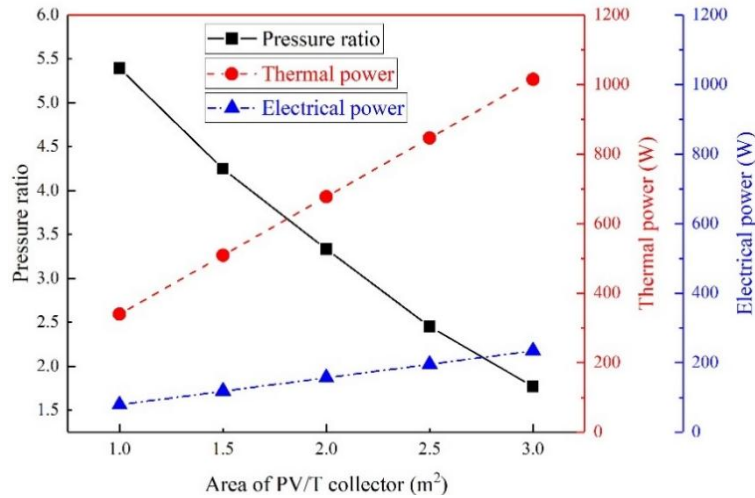


Fig. 22. Influence of the area of PV/T collector on pressure ratio, thermal and electrical power.

As shown in Fig. 23, the mass flow rate of refrigerant will increase when the area increases, while the consumption power of compressor will increase when the area is below 1.5 m² and decrease when the area is over 1.5 m². The mass flow rate of refrigerant will increase because the latent heat and heat capacity of refrigerant are the same when more heat is transferred to the refrigerant. The heat absorbed by the PV/T panel and mass flow rate of refrigerant are low, thus the compressor consumes less electricity to compress the refrigerant vapor. With the increase of the area, the mass flow rate mounts resulting in an increase of consumption power. However, the pressure ratio of the compressor will reduce when the area increases over 1.5 m² leading to a lower consumption power.

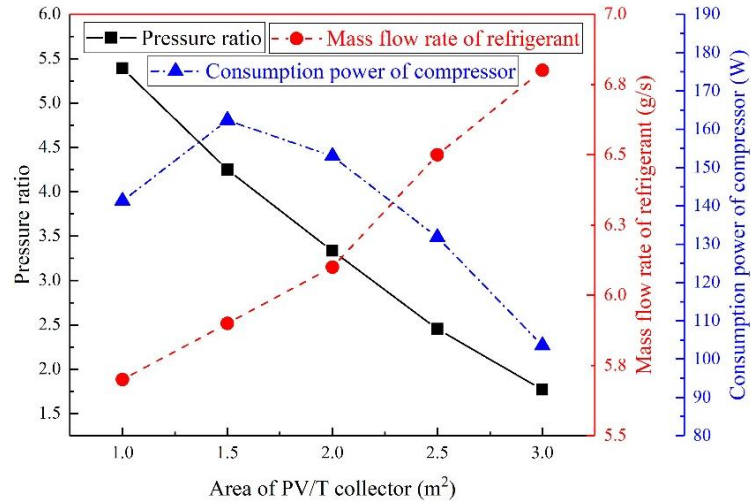


Fig. 23. Influence of the area of PV/T collector on pressure ratio, mass flow rate of refrigerant and consumption power of compressor.

Fig. 24 illustrates the variation curve of output power to grid with the area of PV/T collector. The electrical power generated by PV panels will meet the demand of compressor when the area of PV/T collector is 2 m². Moreover, the PV cells start to produce electricity to power grid when the area is over 2 m² which means a larger PV/T panel is better for the system performance under the same system conditions.

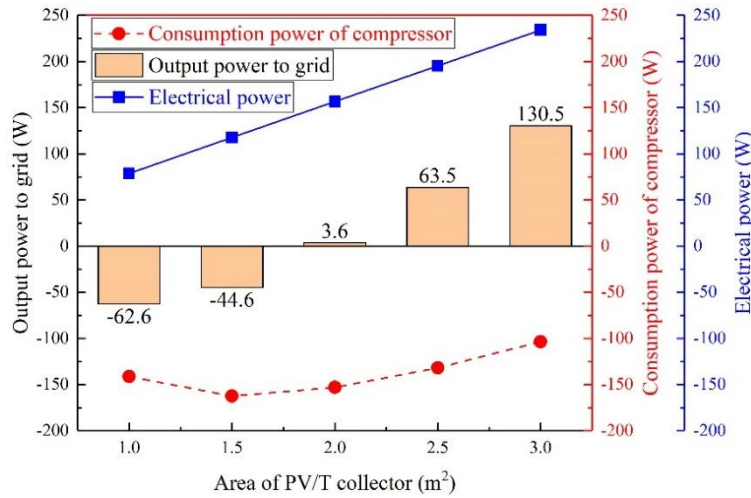


Fig. 24. Influence of area of PV/T collector on electrical power, consumption power of compressor and output power to grid.

5.5 Feasibility analysis of the system

Nowadays, the Chinese government promotes the policy of using electricity for residential heating instead of burning coal for heating in northern China to reduce carbon dioxide emissions. The solar PV/T heat pump coupled with build-in PCM heat storage system is suitable for residential heating due to its advantages: (1) high efficiency; (2) low energy consumption; (3) stable residential heating supply; (4) zero carbon emissions. Table. 4 presents the typical operating conditions and parameters of the system. It is a typical spring/autumn day in northern China.

534

Table. 4. Typical operating conditions and parameters of the system.

Parameters	Nomenclature	Value	Unit
Solar radiation intensity	I	600	W/m^2
Sunshine duration	t_s	8	hour
Ambient temperature	T_a	15	$^{\circ}\text{C}$
Wind speed	v_{wind}	1.5	m/s
Area of the collector	A	20	m^2
Packing factor	β_p	1	[-]
Heating area	A_{ha}	100	m^2
Heat loss per square meter	P_L	50	W/m^2
Filling volume of the PCM	V_{PCM}	0.57	m^3
External diameter of the inside pipe	D_I	0.012	m
Internal diameter of the inside pipe	d_I	0.010	m
External diameter of the outside pipe	D_2	0.074	m
Internal diameter of the outside pipe	d_2	0.072	m
Length of the PCM heat exchanger	L_{hx}	164	m

535

536

537

538

539

540

541

542

543

544

545

546

Table. 5 presents the simulation performance indices of the system under typical day conditions. The PV/T collector can transfer 213.9 MJ heat from the ambient to the PCM heat exchanger, and the heat will be stored in phase change materials and concrete. The build-in PCM heat storage can release the heat for 10 hours at 5.94 kW during the night while the heat loss power of 100 m^2 area is 5 kW. During autumn, winter and early spring in northern China, the heating system is necessary to keep indoor temperature above 20 $^{\circ}\text{C}$. Thus, the system can achieve the heating needs of the users and keep the indoor temperature steady. Meanwhile, the system can output 21.4% (2.79 kWh) of the power generated by PV panels to the grid while 78.6% of it consumed by the compressor. The heating COP of the system is 5.79, and the overall efficiency is 75.49%.

Table. 5. Simulation performance indices of the system under typical day conditions.

Parameters	Value	Unit
Total heat storage	213.9	MJ
Photovoltaic power	1.63	kW
Photovoltaic efficiency	17.77	%
PV/T thermal efficiency	55.76	%
Heating COP	5.79	[-]
Overall efficiency	75.49	%
Cumulative power generation	13.05	kWh
Consumption power of compressor	10.26	kWh
Output power to grid	2.79	kWh
Temperature range of underfloor heating	22-31	$^{\circ}\text{C}$
Heating power at night	5.94	kW
Heat loss power	5.00	kW
Heating hour	10.00	hour

547

548

Table. 6 illustrates the comparison of cost between the proposed system and conventional air

conditioning system. The operating cost of the proposed system is under zero because users could sell spare electricity to power grid and get profit. Fig. 25 shows the cost variation curves of these two systems. The initial cost of the proposed system is much higher than conventional air conditioning system due to the underfloor heating equipment and PV/T panels, etc. However, the air conditioning system consumes a lot of electricity during the night for heating supply. Thus, the cost of these two systems will be the same after about 4 years, and the cost of proposed system keeps reduce while the cost of air conditioning system still climbs. Moreover, underfloor heating system which using radiative heating is more comfort and silence for users than air conditioner.

Table 6. Cost comparison between the proposed system and conventional air conditioning system.

Heating system	Initial cost (¥)	Operating cost (¥/year)	Maintenance cost (¥/year)
Proposed system	22000	-764	550
Air conditioning system	4500	4024	225

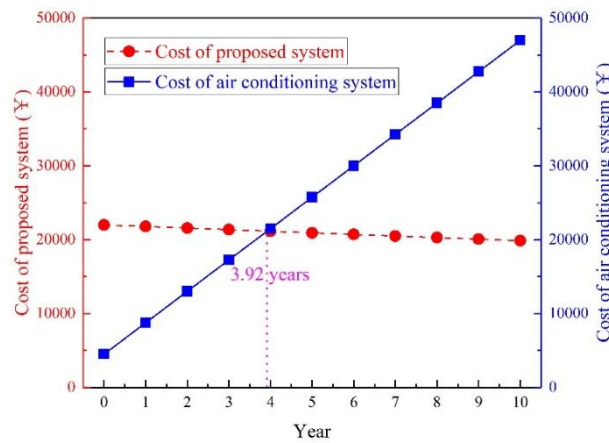


Fig. 25. Cost variation curves of proposed system and air conditioning system.

6 Conclusion

A building-coupled cogeneration system using solar PV/T heat pump and build-in PCM heat storage is proposed in this paper. The mathematical model of the system is established and verified to analyze the system performance under different conditions. The main conclusions can be drawn as follows:

(1) The temperature of underfloor heating which using build-in PCM heat storage can reach 22 °C to 31 °C after 39 hours when the circulating water is 40 °C which is stable and suitable for residential heating.

(2) The heating COP can reach 6.6 which is 94% higher than conventional air conditioning system when solar radiation intensity is 600 W/m², ambient temperature is 25 °C, wind speed is 1.5 m/s and area of PV/T collector is 2 m² while the electrical, thermal and overall efficiencies are 17.05%, 56.43% and 73.87%, respectively.

(3) A 2 m² PV/T panel can meet the power demand of the system and heating demand of a 10 m² room when the solar radiation intensity is 500 W/m². Moreover, the PV/T panel can output electricity to power grid if the panel area is bigger than 2 m² or solar radiation intensity is higher

than 500 W/m^2 .

The mathematical model established in this paper can also be used to analyze and optimize the solar PV/T heat pump system. However, the mathematical model of this system is for stable working conditions instead of transient. The establishment of dynamic model is needed for further predict and analyze accurately of solar assisted heat pump system under dynamic working conditions.

Acknowledgements

This research work is funded by the International Research Cooperation Program of Shanghai (Grant No. 18160710500).

Nomenclature:

Symbols

A	area (m^2)
W	width of the PV/T collector/evaporator (m)
L	length of the PV/T collector/evaporator (m)
ΔH	latent heat (kJ/kg)
h	heat transfer coefficient ($\text{W/m}^2\cdot\text{K}$)
U	heat loss coefficient ($\text{W/m}^2\cdot\text{K}$)
C_p	specific heat at constant pressure (kJ/kg·K)
d	inner diameter (m)
D	external diameter (m)
t/T	temperature (K)
I	solar radiation intensity (W/m^2)
Q	heat transfer rate (W)
F	collector efficiency (-)
R	thermal resistance ($\text{m}^2\cdot\text{K/W}$)
Re	Reynolds number (-)
Ra	Rayleigh number (-)
Pr	Prandtl number (-)
v	wind speed (m/s)
m	mass flowrate (kg/s)
g	gravitational acceleration (m/s^2)
p	pressure (kPa)
P	power (W)
V	volume flow rate (m^3/h)

Greek symbols

δ	thickness (m)
τ	transmittance (-)

	a	absorption ratios (-)
	β	packing factor (-)
	ε	emissivity (-)
	κ	thermal conductivity (W/m·K)
	$\bar{\sigma}$	Stefan-Boltzmann constant (-)
	ρ	density (kg/m ³)
	λ	compressor volumetric efficiency (-)
	η	efficiency (-)
	χ	polytropic index (-)
591		
592	Subscripts	
	p,pv	PV cells
	g,c_1	external glass cover
	c/c_2	PV-glazing cover
	$conc$	concrete
	EVA	EVA grease
	PCM	phase change material
	mel	melting point
	ref	refrigerant
	b	baseboard
	cv	convection
	rd	radiation
	rb	roll-bond panel pipe
	a	ambient
	l	liquid
	L	lost
	rc	reference
	e	electrical
	ei	electrical insulation
	u	uesful
	th/R	thermal
	tp	two-phase flow
	ove	oveall
	abs	absorb
	hp	heat pipe
	sh	superheated
	v	vapor
	$cond$	condensation
	eva	evaporation
	ot	outer pipe
	eq	equivalent
	hx	heat exchanger
	dis	discharge
	suc	suction

<i>in</i>	inlet
<i>out</i>	outlet
<i>cw</i>	circulating water

593

594 **References:**

- 595 2019. Review and outlook of world energy development, Non-Fossil Energy Development in China.
 596 pp. 1-36.
- 597 Ahn, J.-G., Kim, J.-H., Kim, J.-T., 2015. A Study on Experimental Performance of Air-Type PV/T
 598 Collector with HRV. *Energy Procedia* 78, 3007-3012.
- 599 Al-Waeli, A.H.A., Sopian, K., Kazem, H.A., Chaichan, M.T., 2017. Photovoltaic/Thermal (PV/T)
 600 systems: Status and future prospects. *Renewable and Sustainable Energy Reviews* 77, 109-130.
- 601 Cabeza, L.F., Castell, A., Barreneche, C., de Gracia, A., Fernández, A.I., 2011. Materials used as
 602 PCM in thermal energy storage in buildings: A review. *Renewable and Sustainable Energy Reviews*
 603 15(3), 1675-1695.
- 604 Caetano, N.S., Mata, T.M., Martins, A.A., Felgueiras, M.C., 2017. New Trends in Energy
 605 Production and Utilization. *Energy Procedia* 107, 7-14.
- 606 Del Amo, A., Martínez-Gracia, A., Bayod-Rújula, A.A., Cañada, M., 2019. Performance analysis
 607 and experimental validation of a solar-assisted heat pump fed by photovoltaic-thermal collectors.
 608 *Energy* 169, 1214-1223.
- 609 Diallo, T.M.O., Yu, M., Zhou, J., Zhao, X., Shittu, S., Li, G., Ji, J., Hardy, D., 2019. Energy
 610 performance analysis of a novel solar PVT loop heat pipe employing a microchannel heat pipe
 611 evaporator and a PCM triple heat exchanger. *Energy* 167, 866-888.
- 612 Fayaz, H., Rahim, N.A., Hasanuzzaman, M., Rivai, A., Nasrin, R., 2019. Numerical and outdoor
 613 real time experimental investigation of performance of PCM based PVT system. *Solar Energy* 179,
 614 135-150.
- 615 Fiorentini, M., Cooper, P., Ma, Z., Robinson, D.A., 2015. Hybrid Model Predictive Control of a
 616 Residential HVAC System with PVT Energy Generation and PCM Thermal Storage. *Energy*
 617 *Procedia* 83, 21-30.
- 618 Hosseinzadeh, M., Sardarabadi, M., Passandideh-Fard, M., 2018. Energy and exergy analysis of
 619 nanofluid based photovoltaic thermal system integrated with phase change material. *Energy* 147,
 620 636-647.
- 621 Hu, J., Chen, W., Yang, D., Zhao, B., Song, H., Ge, B., 2016. Energy performance of ETFE cushion
 622 roof integrated photovoltaic/thermal system on hot and cold days. *Applied Energy* 173, 40-51.
- 623 Huang, B.J., Lee, C.P., 2004. Long-term performance of solar-assisted heat pump water heater.
 624 *Renewable Energy* 29(4), 633-639.
- 625 Huide, F., Xuxin, Z., Lei, M., Tao, Z., Qixing, W., Hongyuan, S., 2017. A comparative study on
 626 three types of solar utilization technologies for buildings: Photovoltaic, solar thermal and hybrid
 627 photovoltaic/thermal systems. *Energy Conversion and Management* 140, 1-13.
- 628 Jankowski, N.R., McCluskey, F.P., 2014. A review of phase change materials for vehicle component
 629 thermal buffering. *Applied Energy* 113, 1525-1561.
- 630 Kazemian, A., Salari, A., Hakkaki-Fard, A., Ma, T., 2019. Numerical investigation and parametric
 631 analysis of a photovoltaic thermal system integrated with phase change material. *Applied Energy*
 632 238, 734-746.

- Keček, D., Mikulić, D., Lovrinčević, Ž., 2019. Deployment of renewable energy: Economic effects on the Croatian economy. *Energy Policy* 126, 402-410.
- Kuik, O., Branger, F., Quirion, P., 2019. Competitive advantage in the renewable energy industry: Evidence from a gravity model. *Renewable Energy* 131, 472-481.
- Kuznik, F., Virgone, J., Roux, J.-J., 2008. Energetic efficiency of room wall containing PCM wallboard: A full-scale experimental investigation. *Energy and Buildings* 40(2), 148-156.
- Li, G., Pei, G., Ji, J., Yang, M., Su, Y., Xu, N., 2015. Numerical and experimental study on a PV/T system with static miniature solar concentrator. *Solar Energy* 120, 565-574.
- Ma, Y., 2013. Analysis of Electrical Efficiency for Positive Displacement Refrigerant Compressor. *Journal of Refrigeration*.
- Mojumder, J.C., Chong, W.T., Ong, H.C., Leong, K.Y., Abdullah Al, M., 2016. An experimental investigation on performance analysis of air type photovoltaic thermal collector system integrated with cooling fins design. *Energy and Buildings* 130, 272-285.
- Nahar, A., Hasanuzzaman, M., Rahim, N.A., 2017. A Three-Dimensional Comprehensive Numerical Investigation of Different Operating Parameters on the Performance of a Photovoltaic Thermal System With Pancake Collector. *Journal of Solar Energy Engineering* 139(3), 031009.
- Othman, M.Y., Hamid, S.A., Tabook, M.A.S., Sopian, K., Roslan, M.H., Ibarahim, Z., 2016. Performance analysis of PV/T Combi with water and air heating system: An experimental study. *Renewable Energy* 86, 716-722.
- P. Hartnett, J., M. Rohsenow, W., 1973. *Handbook of Heat Transfer*.
- Paolo Frankl, S., 2010. *Technology Roadmap: Solar Photovoltaic Energy*.
- Pereira da Cunha, J., Eames, P., 2016. Thermal energy storage for low and medium temperature applications using phase change materials – A review. *Applied Energy* 177, 227-238.
- Pietrosemoli, L., Rodríguez-Monroy, C., 2019. The Venezuelan energy crisis: Renewable energies in the transition towards sustainability. *Renewable and Sustainable Energy Reviews* 105, 415-426.
- Qiu, Z., Zhao, X., Li, P., Zhang, X., Ali, S., Tan, J., 2015. Theoretical investigation of the energy performance of a novel MPCM (Microencapsulated Phase Change Material) slurry based PV/T module. *Energy* 87, 686-698.
- R. Turns, S., 2006. *Thermodynamics. Concepts and applications*.
- Stojanović, B., Akander, J., 2010. Build-up and long-term performance test of a full-scale solar-assisted heat pump system for residential heating in Nordic climatic conditions. *Applied Thermal Engineering* 30(2-3), 188-195.
- Tsai, H.-L., 2015. Modeling and validation of refrigerant-based PVT-assisted heat pump water heating (PVTA-HPWH) system. *Solar Energy* 122, 36-47.
- Wolf, M., 1976. Performance analyses of combined heating and photovoltaic power systems for residences. *Energy Conversion* 16(1), 79-90.
- Zhou, C., Liang, R., Zhang, J., Riaz, A., 2019. Experimental study on the cogeneration performance of roll-bond-PVT heat pump system with single stage compression during summer. *Applied Thermal Engineering* 149, 249-261.

Conflict of Interest

We declare that there are no conflicts of interest in the work we submitted.



Shanghai Jiao Tong University

Prof. Yanjun Dai, Engineering Research Center of Solar Power and Refrigeration, Dongchuan Road 800#, Shanghai, 200240, P.R. China.

Tel: 8621-3420-4358 Fax: 8621-3420-6814 E-mail: yjdai@sjtu.edu.cn

Dear Editor,

Enclosed please find our manuscript entitled: “**Performance analysis of solar assisted heat pump coupled with build-in PCM heat storage based on PV/T panel**” (written by J. Yao, H. Xu, Y. J. Dai *, M. J. Huang), for possible publication in **SOLAR ENERGY**. The paper has been prepared according to the guidelines listed in the “Guide for Authors-Contents List”. The paper has been received by ‘*1st International Conference for Global Chinese Academia on Energy and Built Environment*’, and the number of **Abstract** is **2019-601**.

We appreciate your consideration of our manuscript, and look forward to receiving comments from the reviewers. Please acknowledge receipt of this manuscript at your convenience, and let us know if you need any further information.

Thanks for your consideration.

Sincerely,

A handwritten signature in black ink, reading 'Yanjun Dai'.

Prof. Yanjun Dai (Y.J. Dai)

Engineering Research Center of Solar Power and Refrigeration

Shanghai Jiao Tong University

Shanghai, 200240, P.R. China